Energy Advances

ROYAL SOCIETY OF CHEMISTRY

REVIEW ARTICLE

View Article Online
View Journal | View Issue

Cite this: *Energy Adv.*, 2025, 4, 364

Impact of powder and electrode ALD coatings on the performance of intercalation cathodes for lithium–ion batteries†

Princess Stephanie Llanos, Alisa R. Bogdanova, Filipp Obrezkov, Nastaran Farrahi and Tanja Kallio *

Received 31st October 2024,
Accepted 2nd January 2025

DOI: 10.1039/d4ya00583j

rsc.li/energy-advances

The desire to obtain higher energy densities in lithium–ion batteries (LIBs) to meet the growing demands of emerging technologies is faced with challenges related to poor capacity retention during cycling caused by structural and interfacial instability of the battery materials. Since the electrode–electrolyte interface plays a decisive role in achieving remarkable electrochemical performance, it must be suitably engineered to address the aforementioned issues. The development of coatings, particularly on the surface of cathode materials, has been proven to be effective in resolving interfacial issues in LIBs. The use of atomic layer deposition (ALD) over other surface coating techniques is advantageous in terms of coating uniformity, conformity, and thickness control. This review article provides a summary of the impact of various ALD-engineered surface coatings to the cycling performance of different intercalation cathode materials in LIBs. Since ALD allows coating development on complex substrates, this article provides a comprehensive discussion of coatings formed directly on a powder active material and composite electrode. Additionally, a perspective regarding the fundamental deposition parameters and electrochemical testing data to be reported in future research is provided.

1 Introduction

The increasing global demand for energy has led to numerous efforts on research and development of sustainable sources, to address climate change and rapid depletion of limited natural resources.[1] Renewable energy sources (RES), such as solar and wind energies, have emerged as essential alternatives to reduce reliance on carbon-based fuels, thereby lowering greenhouse gas emissions. However, the intermittency of RES drives the need for effective energy storage technologies, to address fluctuating supply flow and ensure that sufficient energy is available when energy demand is high.[2] Thus, the development of energy storage systems plays a key role in ensuring uninterrupted power supply for daily consumption while addressing environmental issues.[3–6]

In recent years, lithium–ion batteries (LIBs) have been the leading energy storage technology employed in several applications including portable electronics, transportation, and electrical power grid. The dominance of LIB in these applications, compared with other rechargeable batteries, is rooted in its higher gravimetric and volumetric energy densities.[4,7] However, there is still a need to enhance these features to meet the rising performance expectations of portable devices and electric vehicles. In the matter of grid integration of RES, stability and safety are the critical considerations.[3,8,9] Thus, next-generation LIBs are expected to deliver higher capacity, faster charging times, and improved cycling lifetime without overlooking cost and safety.[6–8]

Since the overall battery characteristics depend on the choice of cathode, anode, and electrolyte materials, it is sensible to develop innovative materials and techniques with favorable electrochemical performance.[10–14] Various materials have been explored and developed to reach a higher energy density output. However, achieving a long-term cycling stability still remains to be a challenge. The instability is driven by the degradation of the electrodes and electrolyte components during the charge and discharge operations.[15–17] The degradation mechanisms are identified as either mechanical or electrochemical including substantial electrode volume variation (especially for anode materials),[18,19] cathode material dissolution,[20–22] gas evolution,[23] and electrolyte decomposition which leads to the formation of a solid–electrolyte interface (SEI)[24–26] and a cathode-electrolyte interface (CEI)[27–29] on the surface of the anode and cathode materials, respectively. All of these issues lead to active material

Department of Chemistry and Materials Science, School of Chemical Engineering, Aalto University, Espoo, 02150, Finland. E-mail: tanja.kallio@aalto.fi

† Electronic supplementary information (ESI) available: Electrochemical performance data of selected studies. See DOI: https://doi.org/10.1039/d4ya00583j

loss and impedance growth, resulting in capacity loss and poor LIB performance.[7,9]

The choice of positive electrode or cathode material has a strong influence on the overall LIB performance. Aside from being the heaviest and most costly component, the cathode mostly determines the energy density of the cell.[7,30,31] Moreover, the properties of the CEI can significantly influence the cycling stability. The drastic non-uniform growth of this interfacial layer creates an additional barrier to Li^+ mobility during deintercalation and intercalation processes, increasing the overall resistance within the cell.[5,32,33] On the other hand, a stable CEI layer can prevent the continuous unwanted interfacial side reactions between the cathode and electrolyte.[34] With these in mind, the electrode–electrolyte interface must be suitably designed to help achieve remarkable cycling performance.[35,36] Surface modification *via* development of a coating layer on the surface of the cathode has been proven to be effective in resolving the interfacial issues in LIBs.[11,33] To promote longer cycling lifetime, while maintaining high energy density, a stable and ionically conductive coating is preformed on the surface of the cathode to act as a protective or a sacrificial layer and protect the bulk electrode material from the aforementioned degradation phenomena.[37,38]

Different materials can be utilized as an artificial CEI, depending on the nature of the cathode material.[39] However, the following properties are highly desired in the preformed surface coatings: (1) uniform formation, (2) continuous and conformal, (3) highly ionic and/or electronic conductive, (4) mechanically stable to accommodate large volume changes, and (5) electrochemically/chemically stable in a wide potential window.[40–42] Surface coating development on cathode materials has been demonstrated by a number of techniques including solution-based precipitation, sol–gel, pulsed layer deposition (PLD), chemical vapor deposition (CVD), and atomic layer deposition (ALD).[11,43] Among these techniques, ALD has emerged as a highly effective method to engineer the surface of cathode materials. It is a gas-phase thin film deposition technique that can precisely control coating thickness, a parameter which significantly impacts Li^+ movement within the interface. Overly thick coatings can impede charge transfer while exceedingly thin coatings are not able to protect the bulk material particles from the damaging side reactions with the electrolyte. Moreover, the conformal feature of ALD ensures complete surface coverage during deposition.[6,10,30,32,34,44]

A number of review articles have previously tackled the utilization of ALD in different energy conversion and storage technologies such as materials for catalysis, supercapacitors, fuel cells, solar cells, and batteries.[14,17,45–48] In addition to modifying the electrode–electrolyte interface, the application of ALD in LIBs also extends to the synthesis of active electrode materials and solid-state electrolyte.[6,10,17,30,33,44,49,50] The use of ALD in developing artificial CEI have been broadly studied. To some extent, the influence of these ALD-based surface coatings on the electrochemical performance of the cathode has been discussed. Lee *et al.*[6] evaluated the performance of battery materials fabricated *via* powder ALD, Wang *et al.*[44] gave a summary of working mechanisms of recently studied ALD coatings for layered oxide cathodes, while Jin *et al.*[24] provided an overview of the improvement mechanisms of ALD thin film coatings on different LIB components. However, there is limited discussion and lack of in-depth analysis on the impact of the different types of ALD coatings on the electrochemical performance of the modified cathode. To date, multiple surface coating materials have been developed using ALD including metal oxides, nitrides, sulfides, fluorides, phosphates, Li-containing mixed oxides, and other complex compounds. Taking into account the numerous types of active materials employed in today's LIB technology, there is a plethora of ALD-related studies with various pairings of cathode material and coating type. Thus, a summary of the optimal coating and parameters (*e.g.* thickness) for each cathode material is beneficial.

In this review, the electrochemical performance, specifically cycling stability and rate capability, of ALD-modified cathode materials in LIBs are extensively discussed and compared. Since most research efforts have been focused on intercalation cathodes, the discussion encompasses layered oxide and spinel types. The difference between powder and electrode ALD processes in enhancing cycling performance is highlighted. Moreover, insights regarding pertinent information that must be presented in ALD-related publications are provided. In light of the rising interest in the role of ALD in LIBs, specifically in the development of artificial CEI, this work provides a comprehensive analysis of coating material performance to guide future ALD-related research on batteries, even beyond LIBs.

1.1 Fundamental principles of ALD

ALD is proven to be an efficient and versatile method to develop different kinds of surface coatings on various types of cathode materials due to its wide range of deposition temperature, allowing fine tuning of the process conditions depending on the substrate material properties. Moreover, the method can be applied on substrates with complex topographies, without sacrificing the uniformity of the coating.[14,49–51] Fig. 1 shows a schematic diagram of a typical ALD process of Al_2O_3 which involves a four-step cycle of alternating pulsing and purging of precursor materials.

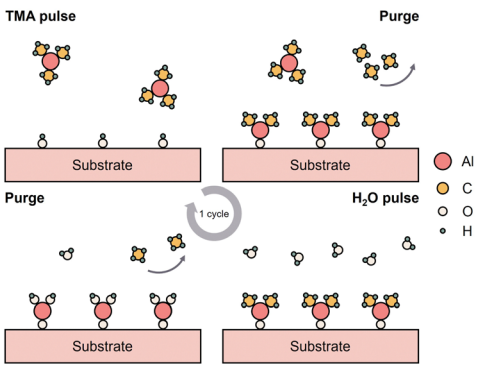

Fig. 1 Schematic diagram of one ALD cycle of Al_2O_3 deposition using trimethylaluminum (TMA) and H_2O as precursors.

The four-step ALD cycle includes: (1) pulsing the first precursor to trigger surface reaction with the reactive sites on the substrate, forming the intermediate and byproducts, (2) purging *via* inert gas to remove residual precursor and reaction byproducts, (3) pulsing of the second precursor to react with the intermediate and generate the desired coating material and new reaction sites, and (4) repeated purging process.[45–47] The self-limiting surface reactions during precursor pulsing is the key feature that allows the method to form one atomic layer at a time. Thus, the coating thickness can be controlled by the number of ALD cycles utilized during the deposition process.[30,48] George[52] have provided a thorough discussion on the fundamental principles of ALD.

1.2 Intercalation-based cathodes

Since the commercialization of the first cathode for LIBs in 1991, various other types of materials have been studied. Recently, intercalation cathodes are commercially favored due to their high capacity and wide operating voltage range, which results in higher energy density.[53,54] Thus, it comes as no surprise that most ALD-related studies on LIB centered on improving the cycling stability of intercalation cathodes, specifically layered and spinel types. Since these cathode materials serve as the substrate during ALD coating development, it is important to understand their attributes.[51] The following discussion provides a brief overview of the properties of the cathode materials examined in this review.

The layered metal oxide $LiCoO_2$ (LCO) is a widely used cathode, especially in portable electronics. However, despite its high theoretical capacity and good Li^+ conductivity, the practical capacity of LCO is limited to 140 mA h g^{-1} due to structural instability at a highly delithiated state.[7] Other drawbacks include high cost and toxicity, mainly due to the presence of Co.[37,55] The ternary layered oxide $LiNi_xMn_yCo_{1-x-y}O_2$ (NMC) combines the advantages of other layered metal oxide-based compounds such as $LiNiO_2$ and $LiMnO_2$. It is a good electrode candidate for LIB due to its high capacity and wide working potential window.[11] In recent years, Ni-rich NMC ($LiNi_xMn_yCo_{1-x-y}O_2$; $x \geq 0.3$), such as $LiNi_{0.8}Mn_{0.1}Co_{0.1}O_2$ (NMC811), is gaining attention due to its higher specific energy and reduced cost, which are highly desirable properties for electric vehicle battery systems. However, it suffers from drastic capacity fade worse than lower Ni content NMC due to irreversible structural changes, oxygen evolution, and parasitic side reactions with electrolyte at higher state of charge (SOC).[44,54,56] Researchers developed Li-rich layered oxides (LLO), such as Li_2MnO_3 to achieve significantly higher capacity.[54,57] The improved performance is attributed to the presence of extra Li^+ with respect to other layered oxides. However, a rearrangement of the bulk and surface materials results in poor Li^+ mobility and voltage fading. Moreover, the insulating property of Li_2MnO_3 contributes to its poor rate capability.[58,59]

Spinel-type cathode materials include $LiMn_2O_4$ (LMO) and $LiNi_{0.5}Mn_{1.5}O_4$ (LNMO). Aside from its low cost, LMO is a promising cathode type due to its exceptional rate capability which is a result of its three-dimensional host structure for Li^+ extraction and insertion. However, its widespread adoption is constrained by Mn dissolution into the electrolyte which leads to interfacial issues and poor cycle stability.[60–62] LNMO is formed when 25% of Mn is substituted with Ni, with a potential in high energy applications due to its dominant plateau at 4.7 V. However, the elevated operating voltage poses challenges to electrochemical stability since it is outside the electrolyte stability window. Operating at this potential leads to aggressive electrolyte decomposition and formation of CEI, thereby causing poor performance.[63–65]

As briefly discussed, the layered and spinel type cathodes possess inherent promising characteristics but also face numerous drawbacks during cycling operations.[4,7,37,54,55] The role of ALD in addressing the electrochemical and/or mechanical degradation in LCO, NMC, LLO, LMO, and LNMO is analyzed in this work. Due to its layer-by-layer growth mechanism, ALD is capable of depositing films on a wide range of substrate materials with controlled thicknesses. Electrode modification using ALD can then be achieved by either directly coating the cathode active material (CAM) in powder form or by coating the composite electrodes composed of the CAM, conducting agent, and binder on a current collector.[6,51] Throughout this review, the former process is referred to as ''powder ALD'' while the latter procedure is designated as ''electrode ALD''. Based on the literature available, powder ALD has been the more commonly applied approach over the past decade.[66] On the other hand, interest on electrode ALD has been growing in recent years due to the advantages it offers over the former method.[6] Both of these ALD processes are discussed in detail in the following sections.

2 Surface coating by ALD

2.1 Powder ALD

Powder ALD has become a powerful tool over the last two decades, overcoming several obstacles to achieve a conformal coating.[6] The main challenges encountered during individual nanoparticle coating include particle agglomeration and film growth dependency on porous and irregular structure.[67] To address these challenges, advanced ALD reactors for powder coating were developed such as fluidized-bed and rotary reactors, coupled with mechanical vibration and agitation.[68–70] Nowadays, the majority of research carried out for enhancing cathode material performance employs such reactors. Fig. 2 illustrates the scheme for powder ALD-based approaches. As seen from the scheme, four main types of surface coatings can be obtained using powder ALD: (1) metal oxide (MO_x), (2) lithiated metal oxide ($Li_xM_yO_z$), (3) post-treated metal oxide, and (4) non-oxide coatings (*e.g.* fluoride, phosphate, organometallic-based).

The main goal in applying various coatings onto CAMs is to improve stability and capacity retention during long term cycling. However, comparing the bare and coated CAMs based on parameters such as capacity decay per cycle (absolute or

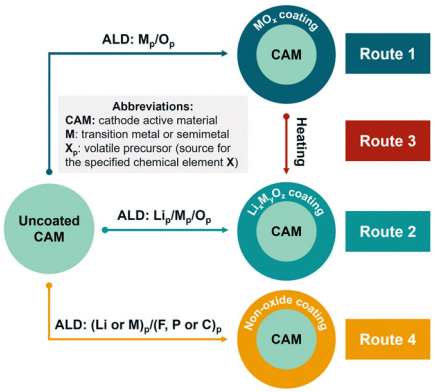

Fig. 2 Scheme of powder ALD-based approaches to obtain a coated CAM categorized by the nature of the coating material.

relative) or overall improvement of this metric does not seem adequate for the cases where absolute value of the specific capacity is low due to the quality of the studied material or peculiarities of test conditions. Therefore, the capacity at the 100th cycle, with current rates ranging from 70 mA g^{-1} (0.5C for LNMO) to 500 mA g^{-1} (2C for most LLO), has been selected as a good figure of merit to compare between different CAMs and coatings to find the best approaches for cathode modification by power ALD. The decision to use the 100th cycle as a point of comparison is conditioned by the fact that most topical articles evaluate the cycling stability until or beyond this point. Studies that reported lower number of cycles have been excluded in the discussion due to limited availability. More importantly, it is challenging to make reliable conclusions about stability with such short cycling duration.

It must be noted that some studies did not directly provide the specific discharge capacity value at the 100th cycle but instead only provided cycling plots. To extract quantitative data needed for the analysis, the plots were analyzed using Web Plot Digitizer (WPD).[71] Aside from specific discharge capacity value, a number of studies did not report the coating thickness. As a result, the number of ALD cycles has been selected as the comparative criterion to analyze electrochemical performance across different studies. Although this approach may not account for all variations in coating thickness due to differences in setups, it provides a practical framework for comparative analysis given the data available. Moreover, due to the complex correlation between different ALD parameters (*e.g.* deposition temperature, pulse rate, *etc.*), the optimal ALD conditions for developing the coating materials are excluded in the discussion and can be found elsewhere.[72]

As discussed in Section 1.2, recent publications related to powder ALD have been primarily focused on layered and spinel type CAMs. Due to the popularity of powder ALD as a coating technique, there is a large collection of related articles (especially for NMC materials) available. The discussion of all of them hinders the systematization of existing knowledge and makes visual representation of the data impractical. Therefore, in this section, the analysis of available data is primarily based on the coating types depicted in Fig. 2, centering on half-cell setup. Considering the large number of dataset available related to Al_2O_3 as a coating, a separate section is dedicated to the discussion of its impact on different types of CAMs.

2.1.1 Aluminum oxide coating. Nowadays, Al_2O_3 is perhaps the most explored ALD coating due to the moderate temperatures employed during deposition and its lower cost compared to other coating materials. Despite its relatively low ionic conductivity and electrically insulating nature,[73] Al_2O_3 coating has been proven to enhance the performance of cathode materials in LIBs.[21,22,42,60,64,74–118] Fig. 3 illustrates the 100th cycle discharge capacity of studies which report the best cycling performance for intercalation CAMs coated with varying thicknesses (*i.e.* number of ALD cycles) of Al_2O_3. The corresponding electrochemical performance data for selected best performing samples during cycling at room temperature in a half-cell configuration are listed in Table 1. As stated earlier, not all studies have provided the thickness of the formed Al_2O_3 coating. The data (S1, ESI†) indicate that the optimal cycling performance is exhibited by CAMs with five or less ALD cycles of Al_2O_3. As expected, the discharge capacities at the 100th cycle increases as the discharge current decreases, regardless of the CAM type.

Interestingly, Hoskins *et al.*[98] reported a non-uniform coating of Al_2O_3 when using a low ALD cycle number. In this study, a non-ALD reaction between the precursors and residual lithium compounds is observed during the first few ALD cycles, which leads to the formation of Li–Al oxide film instead of pure Al_2O_3. Researchers claim that despite the non-uniformity of the $\leq$2-nm thick coating, intercalation pathways are still open for Li^+ transport, while dissolution of the transition metal (TM) oxides in the bulk electrode is restricted. Nonetheless, most of the studies related to the powder ALD coating of CAMs by Al_2O_3 report conformal coating and enhanced cycling stability.[64,74,77,80,85,119]

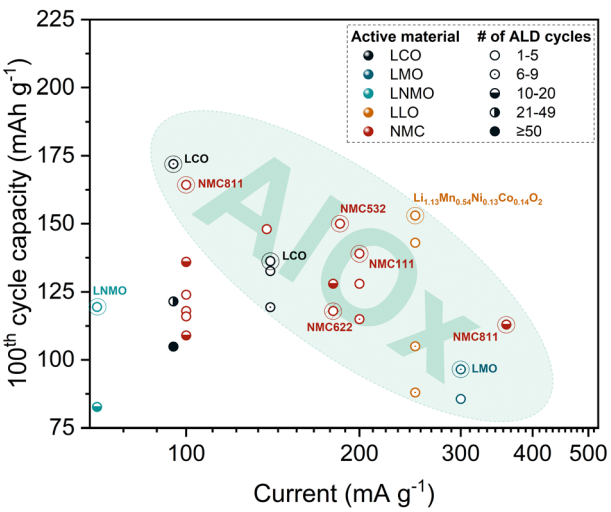

Fig. 3 Specific discharge capacity at the 100th cycle *vs.* discharge current for intercalation CAMs coated with Al_2O_3 using various number of ALD cycles. Plot is based on cycling data (S1, ESI†) using Li metal as counter electrode.

Table 1 Electrochemical performance data of selected studies on Al_2O_3-coated CAMs by powder ALD with Li as counter electrode

Active material	ALD cycles	Thickness, nm	Current, mA g^{-1}	1st cycle discharge capacity, mA h g^{-1}	100th cycle discharge capacity, mA h g^{-1}	Ref.
LCO	8	~1	95	185 (▲5%)	172 (▲17%)	77
LCO	4	—	140	153 (■0%)	136 (▲100%)	74
NMC111	2	—	200	153 (▲1%)	139 (▲34%)	96
NMC532	4	0.40	185	182 (▲2%)	150 (▲552%)	110
NMC622	2	—	180	129 (▼8%)	118 (▲26%)	91
NMC811	4	—	100	198 (▼4%)	164 (▲16%)	85
NMC811	10	3.40	360	158 (▲4%)	113 (▲22%)	86
$Li_{1.13}Mn_{0.54}Ni_{0.13}Co_{0.14}O_2$	2	—	250	165 (■0%)	153 (▲410%)	98
LMO	6	0.72	300	102 (No data)	97 (▲23%)	119
LNMO	5	0.60	70	111 (▼10%)	120 (▲1%)	83

The symbol and corresponding percentage refer to the relative change of the reported value with respect to the uncoated CAM (increased ▲, decreased ▼, not changed ■).

In the following sections, the best electrochemical results, in terms of capacity retention, for Al_2O_3 powder ALD-modified CAMs are presented.

2.1.1.1 Al_2O_3 on layered CAMs. At moderate voltages (~4.2 V), only a fraction (~140 mA h g^{-1}) of the theoretical capacity of LCO is utilized.[53] However, applying a higher voltage than 4.2 V in a half-cell causes an irreversible phase transition and surface degradation, resulting in capacity fading.[55] The application of Al_2O_3 on the CAM *via* ALD is one of the most successful methods in promoting LCO cycling stability at high voltages.

As seen in Fig. 3, LCO with a ~1 nm coating thickness exhibits the highest discharge capacity after 100 cycles. Wu *et al.*[77] reported a specific capacity of 172 mA h g^{-1} with a 93% capacity retention after 200 cycles at 3.0–4.5 V for the LCO coated with 8 ALD cycles of Al_2O_3 (CLCO 8), as shown in Fig. 4a. The enhanced cycling stability was further confirmed by the negligible capacity loss from the 100th to 200th cycle for CLCO 8 compared with bare LCO (BLCO). Moreover, CLCO 8 was able to achieve 88% capacity retention compared to 40% of BLCO after 200 cycles at a higher cutoff potential of 4.6 V. The authors claim to achieve the best LCO cycling performance at high cutoff potentials *via* powder ALD compared with other methods, including wet chemistry and sputtering. Based on high-resolution transmission electron microscopy (HRTEM) and X-ray photoelectron spectroscopy (XPS) results, the Al_2O_3 coating layer is reconstructed into Li_3AlF_6 during cycling. This newly formed structure binds more tightly to the LCO surface as compared with direct coating and retains good Li^+ and cycling stability when reacted with electrolyte decomposition products. Moreover, it inhibits surface stripping and shields Co and O from dissolution during cycling.[77]

Jung *et al.*[74] reported Al_2O_3-coated (4 ALD cycles) LCO to deliver 44% higher capacity retention than bare LCO after 100 cycles at 3.3–4.5 V. Similar to the previously discussed work,[77] the enhanced cyclability is attributed to the ability of the ultrathin Al_2O_3 coating to minimize Co dissolution or reduce reactions at the LCO electrode–electrolyte interface. The study also highlighted the electronically insulating property of Al_2O_3 wherein the discharge capacity starts to decrease significantly as the number of ALD cycles increases. This capacity loss stems from the large overpotential induced by the Al_2O_3 layer, as a result of the decreasing electronic conductivity of the coated LCO due to the increase in the coating thickness.

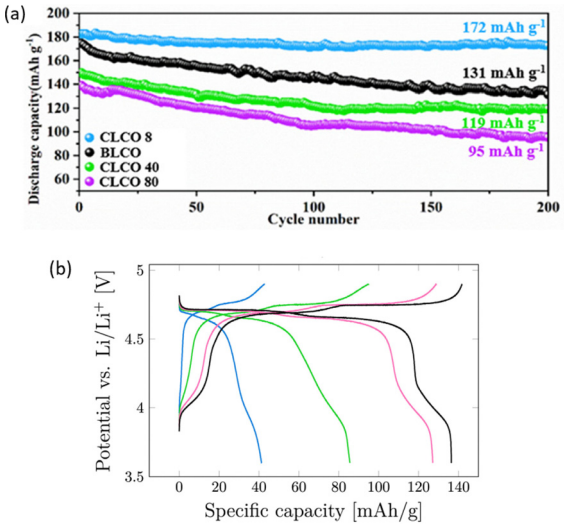

Fig. 4 (a) Cycling performance of the uncoated (BLCO) and Al_2O_3-coated LCO (CLCO) using 8, 40 and 80 ALD cycles at 3.0–4.5 V. Reprinted with permission from ref. 77. Copyright 2022 American Chemical Society; (b) second charge–discharge cycle for the uncoated LNMO (black), 5 (pink), 10 (green), and 20 (blue) ALD Al_2O_3 cycles at C/10. Reprinted from ref. 83. Copyright 2021 The Authors. Published by American Chemical Society. This work is licensed under a Creative Commons Attribution 4.0 CC-BY International License.

Despite the advantages of NMC, this type of a CAM suffers from drastic capacity fading.[120] Several studies have reported the successful application of Al_2O_3 powder ALD in addressing NMC degradation issues, especially ones with higher Ni content. Based on the highlighted region in Fig. 3, a NMC material with a coating of less than 5 ALD cycles exhibits the highest discharge capacity of 164 mA h g^{-1} after 100 cycles. Gao *et al.*[85] reported enhanced cycling performance of Al_2O_3-coated (~0.5 nm) NMC811 in an extended potential window of 2.5–4.5 V. The impressive results were attributed to a more stable interface between the electrolyte and the Al_2O_3-coated CAM particles. Even when the coated material is cycled at higher

C-rates, specifically at 2C, the Al_2O_3 ALD coating is still efficient in improving the cycling stability. For example, in the work of Kim *et al.*,[86] NMC811 demonstrated a specific discharge capacity of 113 mA h g^{-1} after 100 cycles at 2C (360 mA g^{-1} in Fig. 3). The reported capacity retention is ~72% when tested at the potential window of 2.8–4.3 V. The authors believe that the ~3.40 nm (10 ALD cycles) coating on the NMC811 CAM can mitigate the side reactions that occur at the electrode–electrolyte interface.

Li *et al.*[110] also hypothesized that the ultrathin Al_2O_3 coating can protect the surface of $LiNi_{0.5}Mn_{0.3}Co_{0.2}O_2$ (NMC532) CAM from electrolyte corrosion during cycling and favorably affects interfacial stability. In their work, the Al_2O_3-coated (~0.40 nm; 4 ALD cycles) NMC532 exhibited 150 mA h g^{-1} after 100 charge–discharge cycles, which corresponds to 82% capacity retention at a high cutoff potential of 4.55 V. On the other hand, the uncoated NMC532 provided only 23 mA h g^{-1} which corresponds to ~12% capacity retention at the same cycling conditions. Based on the Rietveld refinement of X-ray diffraction (XRD) patterns, the coated NMC532 showed lower cation mixing between Ni^{2+} and Li^+ compared to the uncoated NMC532, which could explain the better stability of the modified material. However, the Li^+ diffusion coefficient of the coated NMC532 was lower than the uncoated NMC532 due to the poor Li^+ conductivity of the Al_2O_3.

The effect of Al_2O_3 coating on the Li^+ transport behavior was also investigated in the work of Li *et al.*[91] Based on the electrochemical impedance spectroscopy (EIS) results, the charge transfer resistance (R_{ct}) of $LiNi_{0.6}Mn_{0.2}Co_{0.2}O_2$ (NMC622) coated with 2 ALD cycles of Al_2O_3 is 2.6 times higher than the uncoated NMC622 after the 2nd charge–discharge cycle at 4.5 V *vs.* Li/Li^+. The substantial difference implies that the coating has a limiting effect on the Li^+ transfer at the electrode–electrolyte interface. However, after the 300th charge–discharge cycle, the results are reversed wherein the R_{ct} of the uncoated NMC622 is more than 2 times higher than the Al_2O_3-coated NMC622. This can be attributed to the rapid growth of a CEI layer which acts as a Li^+ barrier on the NMC622 particles, leading to low capacity retention. Indeed, the cycling stability enhancement of Al_2O_3-coated sample has been demonstrated by the higher specific discharge capacity of 118 mA h g^{-1} after 100 cycles (Fig. 3). The capacity retention improved by 24% even at a wide potential window of 3.0–4.5 V.

Riley *et al.*[96] also emphasized the cycling stability benefits of depositing Al_2O_3 coating on $LiNi_{1/3}Mn_{1/3}Co_{1/3}O_2$ (NMC111). The application of 2 powder ALD cycles on NMC111 nanoparticles resulted in a specific discharge capacity of 139 mA h g^{-1} after 100 cycles (Fig. 3), corresponding to ~90% capacity retention in the working potential of 3.0–4.5 V. On the other hand, the bare NMC111 exhibited a lower capacity retention of ~68%. Further increase in the number of cycles resulted in worse cycling performance, indicative of the insulating nature of the Al_2O_3 coating.

LLOs have recently gained the attention of researchers due to their ability to deliver high specific capacities (≥250 mA h g^{-1}) when operated in a wide potential range of 2.0–4.8 V *vs.* Li.[57] However, their commercial use is hindered by poor kinetics and voltage decay upon cycling.[121] As with NMC, powder ALD coating has been applied to address these issues. Hoskins *et al.*[98] reported that by applying 2 ALD cycles of Al_2O_3 on $Li_{1.13}Mn_{0.54}Ni_{0.13}Co_{0.14}O_2$ CAM, a specific discharge capacity of 153 mA h g^{-1} has been achieved after 100 cycles at 1C (250 mA g^{-1} in Fig. 3). The coated LLO CAM exhibited a stable behavior until the 120th cycle while cycling at an upper cutoff potential of 4.8 V. Meanwhile, the LLO CAM coated by 4 ALD cycles of Al_2O_3 delivered about 145 mA h g^{-1} after 100 cycles and showed stable performance until the 160th cycle. In both cases, sub-2 nm thick Al_2O_3 films verified their efficiency in improving the cycling stability of the LLO.

2.1.1.2 Al_2O_3 on spinel CAMs. Mn dissolution and Jahn–Teller (J–T) distortion are considered to be the main factors affecting the cycling performance of LMO, causing continuous capacity fading.[60,62] One of the strategies to deal with TM dissolution is through the application of thin film coating on the CAM powder by ALD. For instance, Luan *et al.*[119] determined the optimal cycling performance of LMO by investigating the impact of varying the Al_2O_3 ALD coating cycles to the battery cycling behavior at 3.4–4.5 V with 300 mA g^{-1} current rate. Based on the results, the study reported 6 Al_2O_3 ALD cycles (~0.72 nm) to be the optimal condition, allowing to reach a capacity of 97 mA h g^{-1} after 100 cycles (Fig. 3). On the other hand, using the same cycling parameters, the specific discharge capacity of the bare LMO at 100th cycle was found to be lower at 79 mA h g^{-1}.

LNMO suffers from TM dissolution and rapid capacity decay in the high operating potential of 4.7 V *vs.* Li.[122] Similar to other CAMs, direct surface coating on the LNMO particles can address the drawbacks limiting its full performance. However, based on literature, the impact of Al_2O_3 coating on LNMO is still ambiguous. While in some cases the presence of a coating results in improved capacity retention compared with a bare CAM,[64,82,83] for some studies Al_2O_3 has negligible impact.[80] To date, the best reported cycling performance of Al_2O_3-coated (0.60 nm; 5 ALD cycles) LNMO *via* powder ALD is a specific discharge capacity of ~120 mA h g^{-1} (Fig. 3) after 100 cycles at 3.6–4.9 V.[83] Although the difference in specific discharge capacity between Al_2O_3-coated and uncoated LNMO after 100 cycles is not significant, it is more pronounced for results after 150 cycles. However, Østli *et al.*[83] claim that for 1-nm (10 ALD cycles) thick coatings, the Al_2O_3-coated samples have high overpotentials (Fig. 4b) and reduced reversible capacity. Authors attribute these findings to the homogeneity of the applied coating, which results in complete coverage of CAM particles and the formation of a Li^+ diffusion barrier.

Based on the findings of the powder ALD studies considered in this analysis, the main impact of Al_2O_3 as a coating is the mitigation of side reactions, especially the suppression of the TM dissolution. As seen in Fig. 3, the coating thickness plays a crucial role in the cycling performance since majority of the most stable Al_2O_3-coated CAMs utilized a low number of ALD cycles (1–5). Conversely, the application of more ALD cycles

does not bring any significant improvement since the insulating nature of a thicker coating deteriorates the electronic and ionic conductivities of the CAM, leading to slower kinetics. Hence, it is crucial to determine the optimal coating thickness.

2.1.2 Other metal oxide-based coatings. In addition to Al_2O_3, various other metal oxides have been investigated as CAM coatings *via* powder ALD. ZnO[74] and ZrO_2[123] have been applied as surface coatings for LCO. A much broader array of oxides has been utilized to coat Ni-rich NMC-type materials: MgO,[124] ZrO_2,[124,125] ZnO,[126] and mixed Al_2O_3–Ga_2O_3 oxides[101] for NMC532; TiO_2,[127] ZrO_2,[128] and WO_3[129] for NMC622; ZrO_2,[16,85] TiO_2,[87] and Ta_2O_5[23] for NMC811; and ZnO[130] for $LiNi_{0.90}Mn_{0.05}Co_{0.05}O_2$. TiO_2,[40,64,131,132] CeO_2,[133] and FeO_x[134–136] have been reported as ALD coatings for spinel-type LNMO while ZnO,[78,137,138] ZrO_2,[78,79,139,140] CeO_2,[79,141] and MgO[20] have been used for LMO. Additionally, ALD coatings such as CeO_2,[142] TiO_2,[102] ZnO,[103,143] and ZrO_2[103] have been applied to $Li_{1.2}Ni_{0.54}Co_{0.13}Mn_{0.13}O_2$, while FeO_x[144] was used to protect another LLO, $Li_{1.13}Mn_{0.54}Ni_{0.13}Co_{0.14}O_2$.

As evidenced by the aforementioned reported coatings, a significant number of studies have focused on the ALD coating of CAMs with various metal oxides other than Al_2O_3, making it impractical to consider each approach and corresponding experimental results in detail. Consequently, similar to the section devoted to powder ALD coating with Al_2O_3, the reported data were analyzed to focus specifically on the most promising materials. Table 2 lists the electrochemical performance of the coating materials investigated in the studies that reported the most impressive cycling results. The data show that for layered oxides such as LCO[123] and Ni-rich NMC,[85,124,128] ZrO_2 obtained *via* 5 ALD cycles or lower has been reported to be the most effective coating. The reliability of powder ALD as a coating method is verified by the comparable results obtained by different research groups.[85,124,128] Additionally, a higher capacity retention was reported for ZrO_2-coated NMC622 after further calcination at a high temperature.[128] Post-treatment of coated CAMs are explored in Section 2.1.3 in more detail.

A comparison of the capacity of the modified CAMs at the 100th cycle is illustrated in Fig. 5, which also includes benchmark results of Al_2O_3 for comparison. The chart shows that there is no significant improvement of specific capacity compared to Al_2O_3-coated CAMs since all the data points reflecting the best results are found in the same highlighted area in the chart. It is noteworthy that Al_2O_3-coated NMC532 exhibited superior performance, whereas Al_2O_3, ZrO_2, and Ta_2O_5-coated NMC811 showed comparable capacities at the 100th cycle.[124] However, the relatively good capacity retention of Ta_2O_5-NMC811 is associated with the quality of the pristine material since the improvement is just 1%.[23] Notably, MgO and ZrO_2 powder ALD coatings significantly improved the discharge capacity at 10C by 190% and 183%, respectively.[124] On the other hand, only 30% of enhancement has been demonstrated by Al_2O_3. The superior rate performance is associated with the higher Li^+ diffusivity for MgO and ZrO_2 coated samples, as shown in Fig. 6.

A notable finding was observed for LLO materials, where the best performance was achieved by $Li_{1.2}Mn_{0.54}Ni_{0.13}Co_{0.13}O_2$

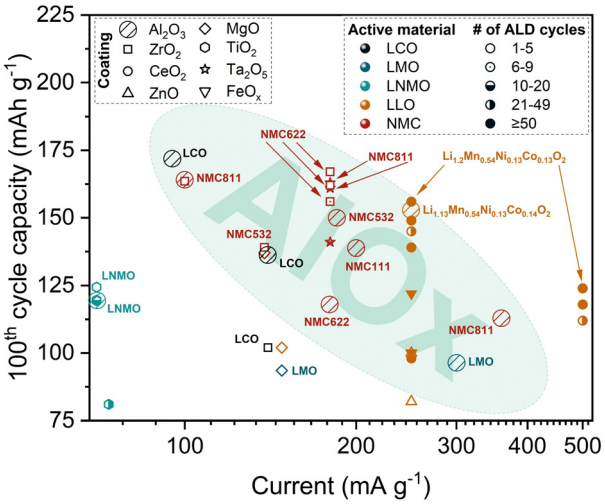

Fig. 5 Specific discharge capacity at the 100th cycle *vs.* discharge current for CAMs coated with different metal oxides *via* powder ALD. The highlighted area signifies the best cycling results obtained with Al_2O_3 coating for comparison.

Table 2 Electrochemical performance data of selected studies on metal oxide-coated CAMs by powder ALD with Li as counter electrode

Active material	Coating material	ALD cycles	Thickness, nm	Current, mA g^{-1}	1st cycle discharge capacity, mA h g^{-1}	100th cycle discharge capacity, mA h g^{-1}	Ref.
LCO	ZrO_2	2	2.56	140	146 (▼2%)	102 (▼13%)	123
NMC532	Al_2O_3	5	—	138	136 (▼13%)	148 (▲16%)	124
NMC532	MgO	5	—	138	155 (▼1%)	137 (▲7%)	124
NMC532	ZrO_2	5	—	138	159 (▲2%)	139 (▲9%)	124
NMC622	ZrO_2	5	1.2	180	172 (▲2%)	167 (▲12%)	128
NMC811	Al_2O_3	4	—	200	198 (▼4%)	164 (▲16%)	85
NMC811	ZrO_2	5	—	200	210 (▲2%)	164 (▲16%)	85
NMC811	Ta_2O_5	2	—	180	190 (▲2%)	163 (▲1%)	23
LMO	MgO	2	—	148	80 (▼38%)	102 (▼12%)	20
LNMO	TiO_2	5	0.2	140	130 (■0%)	124 (▼3%)	131
$Li_{1.2}Mn_{0.54}Ni_{0.13}Co_{0.13}O_2$	CeO_2	50	2.5	250	166 (▲8%)	156 (▲73%)	142
$Li_{1.2}Mn_{0.54}Ni_{0.13}Co_{0.13}O_2$	CeO_2	50	2.5	250	135 (▲5%)	124 (▲49%)	142

The symbol and corresponding percentage refer to the relative change of the reported value with respect to the uncoated CAM (increased ▲, decreased ▼, not changed ■).

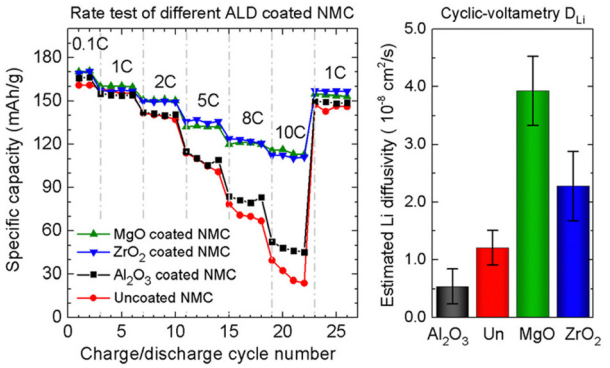

Fig. 6 Rate performance test and Li^+ diffusivity data for uncoated and Al_2O_3, ZrO_2, and MgO-coated NMC532. Reprinted with permission from ref. 124. Copyright 2017 American Chemical Society.

coated with CeO_2.[142] The CeO_2 coating partially solved cell voltage decay, improved substrate conductivity, and provided a barrier against TM dissolution. As a result, the initial capacity increased by ~8% when measured at room temperature. At 55 °C, the coated CAM reported a higher capacity retention (~60.2%) than the uncoated sample after 400 cycles at 1C. Consistent with findings for Al_2O_3, thin film powder coatings (≤1 nm) are predominant for other metal oxides as well. However, CeO_2 is an exception, with an optimal coating thickness reported to be ~2.5 nm (50 ALD cycles).[142] The relatively high number of ALD cycles do not have a detrimental effect to the charge transfer kinetics due to the excellent electrical conductivity of CeO_2. The best cycling performance for metal oxides are selected for further comparison with other types of coating materials, including lithium-containing and non-oxide coatings.

2.1.3 Post-treated metal oxide coatings. As shown in Fig. 2, the formed MO_x coating can be further modified by heating the coated CAM (Route 3). One of the reasons to apply post-annealing to ALD-coated CAMs is to enhance the ionic or electronic conductivity of the material. Analogous to Route 1, Al_2O_3 is the most studied type of a coating material in the post-treated scheme. In the case of Ni-rich NMCs, the subsequent annealing of the Al_2O_3-coated CAM produces a Li-conductive $LiAlO_2$ coating layer.[85,91,110] Li *et al.*[110] compared the electrochemical behavior of Al_2O_3-coated NMC532 and post-treated Al_2O_3-coated NMC532. The post-treated Al_2O_3-coated NMC532 delivered better rate capability and cycling stability. The annealed CAM had higher $LiAlO_2$ content on the particle surface, leading to increased Li^+ conductivity. The improved diffusion kinetics is enabled by the higher Li^+ diffusion coefficient during the charging and discharging processes. The study claims that the enhanced Li^+ transport was due to the rapid H2–H3 phase transition of the post-treated sample revealed by the *in situ* XRD results. In contrast, Gao *et al.*[85] did not observe any improvement in the Li^+ diffusion coefficient for an Al_2O_3-coated and annealed NMC811 CAM. The annealed Al_2O_3-coated NMC811 sample experienced dramatic decrease of Li^+ diffusion coefficient at the H2–H3 transition voltage, which can be associated with a significant shrinkage of the lattice parameter *c* at a highly delithiated state. The sluggish Li^+ mobility implies a negative effect of Al doping to NMC811. However, the ZrO_2 ALD-coated and post-annealed sample demonstrated faster Li^+ transport due to the lower change of lattice parameter *c* compared to the Al_2O_3-coated and post-annealed samples.

Li *et al.*[91] studied the effect of Al_2O_3 powder ALD coating coupled with post-annealing on the Li^+ transport behavior of NMC622 by EIS. The ALD coated and post-treated NMC622 exhibits lower R_{ct} compared with the ALD coated NMC622 without the post treatment. The authors correlate the decrease in R_{ct} after post-annealing with the decline of resistance in Li^+ movement. However, based on the electronic conductivity data, the Al_2O_3-coated CAM with subsequent post-annealing exhibits the lowest conductivity value among all samples. This result is ambiguous since low electronic conductivity leads to charge accumulation at the cathode interface and thereby increases R_{ct}.

Aside from Al_2O_3, post-treatment has been explored for other metal oxide-based powder ALD coatings. For this approach, MgO[20] and ZrO_2[140] coatings have been applied on LMO while iron oxides (FeO_x)[136] have been studied for LNMO. After the powder ALD process, the oxide-coated LMO and LNMO CAMs were heat treated to 300–450 °C for 3 h and 650–700 °C for 4 h in air, respectively. Among Ni-rich NMCs, post-heating treatments ranging between 300–750 °C were employed for NMC622 coated with WO_3[129] and ZrO_2,[128] and for NMC811 coated with ZrO_2.[85] For LLO-based CAMs, post-annealing was reported for FeO_x-coated $Li_{1.13}Mn_{0.54}Ni_{0.13}Co_{0.14}O_2$[144] and ZnO-coated $Li_{1.2}Mn_{0.54}Ni_{0.13}Co_{0.13}O_2$.[143] Both annealing treatments were implemented at high temperatures between 700 to 800 °C, using air for 24 h for the former study while Ar for 30 minutes for the latter work.

Another post-ALD treatment technique is the post-lithiation of the ALD-coated CAM precursor. The work of Cai *et al.*[112] is the only work identified to have reported this type of a strategy, producing Li_5AlO_4-coated NMC811. In the study, the hydroxide precursor, $Ni_{0.83}Co_{0.11}Mn_{0.06}(OH)_2$, was initially coated with Al_2O_3. Afterwards, the Al_2O_3-coated precursor was mixed with LiOH and then sintered at 800 °C for 12 h under an oxygen atmosphere to form the Li_5AlO_4-coated NMC811 CAM. The detailed post-lithiation scheme is illustrated in Fig. 7.

The cycling stability of the CAMs in the aforementioned post-treatment studies are summarized in Fig. 8, which shows the 100th specific discharge capacity for each reported powder ALD coating. Based on the chart, it can be inferred that the post-treated ZnO-coated $Li_{1.2}Mn_{0.54}Ni_{0.13}Co_{0.13}O_2$[143] and post-treated Al_2O_3-coated $Li_{1.08}Ni_{0.22}Co_{0.22}Mn_{0.45}O_2$[111] presented the most promising stability after long term cycling. Similarly, the post-lithiated Al_2O_3-coated $Ni_{0.83}Co_{0.11}Mn_{0.06}(OH)_2$ CAM precursor[112] demonstrated a relatively high specific discharge capacity at a higher current rate. It is recommended to explore these approaches more intensively as the CAM performance exceeds the general trend for the common oxide coated materials.

2.1.4 Li-containing metal oxide coatings. ALD of d- and p-metal oxides is widely employed for coating CAMs due to

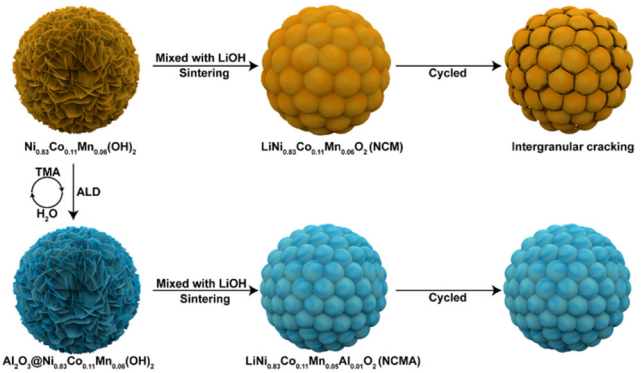

Fig. 7 Schematic diagram of the post-lithiation of coated CAM precursor. Reprinted with permission from ref. 112. Copyright 2023 American Chemical Society.

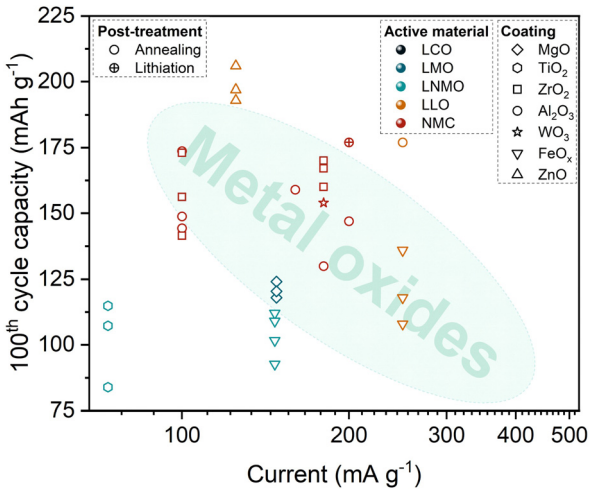

Fig. 8 Specific discharge capacity at the 100th cycle *vs.* discharge current for ALD-coated CAMs with different post-treatment approach. The highlighted area signifies the best cycling results obtained with metal oxide-based coatings for comparison.

several advantages discussed earlier. This practice has led to the development of post-deposition treatment techniques that produce highly efficient Li-containing coatings. However, since 2020,[145] there has been a growing interest in directly coating CAMs with Li-containing mixed oxides *via* ALD using volatile Li precursors. The general approach involves exposing the CAM to ALD supercycles, each consisting of a series of subcycles. These subcycles alternate between the deposition of p- or d-metal oxides and lithium oxide/hydroxide. By carefully balancing the number of subcycles within each supercycle, a uniform Li-containing mixed oxide coating is achieved (Route 2 in Fig. 2).

Although several Li precursors are available for ALD processes,[146] literature predominantly reports the use of lithium *tert*-butoxide (LTB, *t*-BuOLi) for coating CAMs. This trend likely reflects the nascent stage of this research area, where LTB, as a widely recognized and reliable precursor, has been the primary choice. Notably, this method has been successfully applied to Ni-rich and Li-rich NMC. For instance, ALD of lithium

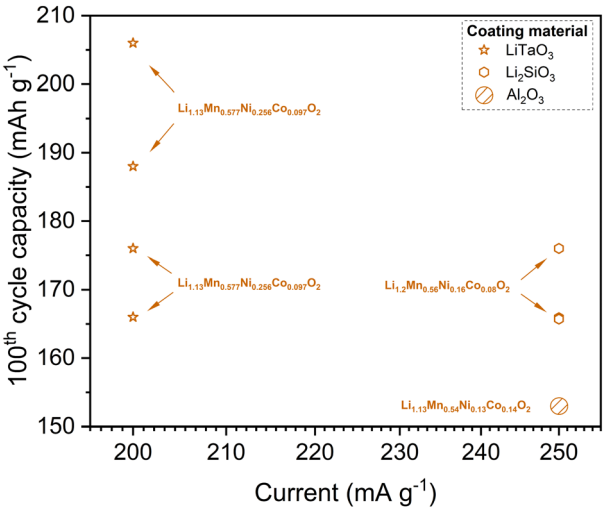

Fig. 9 Specific discharge capacity at the 100th cycle *vs.* discharge current for CAMs coated with different Li-containing mixed oxide coatings *via* powder ALD.

aluminum zinc oxide (LAZO) on $LiNiO_2$ significantly improved the material's specific capacity and stability.[147] The specific capacities for the LAZO-coated $LiNiO_2$ after the 1st and 100th cycles (0.2C, 2.6–4.3 V, 35 °C) were 203 mA h g^{-1} and 182 mA h g^{-1}, respectively, compared to 159 mA h g^{-1} and 116 mA h g^{-1} for the uncoated sample. Other studies have reported the deposition of nanometer-sized lithium zirconium oxide (Li_xZr_y O, LZO) coatings on NMC622[148] and lithium tin oxide ($Li_xSn_yO_z$) on NMC811.[28] However, the variability in experimental conditions (*e.g.* temperature, cycle number, counter electrode material) complicates the direct comparison of cycling results, particularly for Ni-rich NMC. In contrast, Li-rich NMC offer more consistent data for comparison, as shown in Fig. 9.

A pioneering topical study reported $LiTaO_3$-coated $Li_{1.13}Mn_{0.517}Ni_{0.256}Co_{0.097}O_2$ with 3 nm coating thickness (10 ALD supercycles), resulting in a record-high discharge capacity of 206 mA h g^{-1} at 1C ($\geq$200 mA g^{-1}) by the end of 100 cycles.[145] This exceptional performance is attributed to the high ionic conductivity of $LiTaO_3$, a known solid electrolyte compound. Another study[149] reported more modest yet significant improvements using Li_2SiO_3 coatings on $Li_{1.2}Mn_{0.56}Ni_{0.16}Co_{0.08}O_2$, with capacities of 176 mA h g^{-1} after the 100th cycle and 150 mA h g^{-1} after the 300th cycle, making it a strong competitor to modern state-of-the-art materials. At least, these results surpass those of LLO CAMs coated with Al_2O_3 marked in Fig. 9.

A particularly noteworthy study systematically compared the performance of $0.33Li_2MnO_3{\cdot}0.67Li(Ni_{0.4}Co_{0.2}Mn_{0.4})O_2$ coated with Al_2O_3, Li_5AlO_4, and Na_5AlO_4.[113] This research stands out for two reasons: it is the first demonstrated usage of a sodium ALD precursor for CAM coating, and it reported outstanding efficiency across all evaluated parameters. For instance, the electrodes cycled between 2.0–4.7 V at 1C (250 mA g^{-1}) exhibited remarkable specific capacities. Unfortunately, due to the slightly elevated testing temperature (30 °C), the results were not included in Fig. 9. Nonetheless, the study reported at least

400 cycles at different current rates with high capacity values, minimal capacity fade, and reduced crack formation in the coated samples.

Despite these promising results, several challenges associated with the powder ALD of Li-containing mixed oxide coatings remain. The primary challenge is optimizing the supercycle layout to achieve the desired stoichiometry, which can be complex and time-consuming. Incorrectly balanced subcycles may result in coatings that are unstable in air and exhibit poor electrochemical performance. Additionally, the necessity to heat the high-boiling-point Li precursor vessel to high temperatures makes the whole ALD process particularly energy-intensive.

2.1.5 Non-oxide coatings. In addition to d- and p-metal oxides and Li-containing mixed oxides, several other types of powder ALD coatings have demonstrated their effectiveness as protective layers for intercalation CAMs. These include fluorides, phosphates, metals, and coatings produced using the ALD–MLD (atomic layer deposition–molecular layer deposition) method. These non-oxide coatings are grouped together under Route 4 in Fig. 2.

Fluorides have been primarily utilized to protect the surface of LNMO. Notable examples include coatings of LiF,[150] MgF_2,[151] and AlF_3.[152,153] Since all of these studies were performed by the same research group, it is difficult to conclude that fluoride coatings are exceptionally popular, specifically for LNMO. Beyond LNMO, only two studies were published, reporting the powder ALD coating of NMC532[154] and NMC811[155] with AlF_3.

Phosphates form the second notable group of powder ALD coatings, with a broader range of studied CAMs. $FePO_4$[156] and Li_3PO_4, including its mixture with TiO_2,[40] have been employed as coatings for LNMO. Additionally, $AlPO_4$ has been used to coat LLO such as $Li_{1.2}Mn_{0.54}Co_{0.13}Ni_{0.13}O_2$,[157] while Li_3PO_4 served as a barrier layer for Ni-rich NMC materials such as NMC811[158] and $LiNi_{0.9}Mn_{0.05}Co_{0.05}O_2$.[27] However, it is important to note that the specific capacities and stability observed with phosphate-based coatings were generally low, indicating their limited effectiveness as barrier layers.

Metallic coatings have been applied solely to NMC811, which represent a diverse group due to the varying morphologies of the resulting coatings. For example, one study utilized an ALD surface reaction between $Pd(hfac)_2$ and formaldehyde as a reducing agent, resulting in the formation of palladium nanoparticles on the NMC811 surface.[159] Another approach employed the single-precursor atomic surface reduction method with diethyl zinc, which resulted to a uniform zinc coating at 100 °C.[160] When the process temperature was increased to 200 °C, surface doping of the active material particles was observed.

The ALD–MLD method uses a combination of metallic and purely organic compounds as precursors in the deposition process. The organic functional groups are preserved in the final product, leading to the formation of organometallic coatings on the surface of CAMs. For instance, LLO material, $0.35Li_2MnO_3{\cdot}0.65LiNi_{0.35}Mn_{0.45}Co_{0.20}O_2$, was coated with alkylated $Li_xSi_yO_z$ *via* alternating exposures to *t*-$BuMe_2$ SiLi vapor and ozone.[161] In a half-cell configuration, the ALD–MLD coated

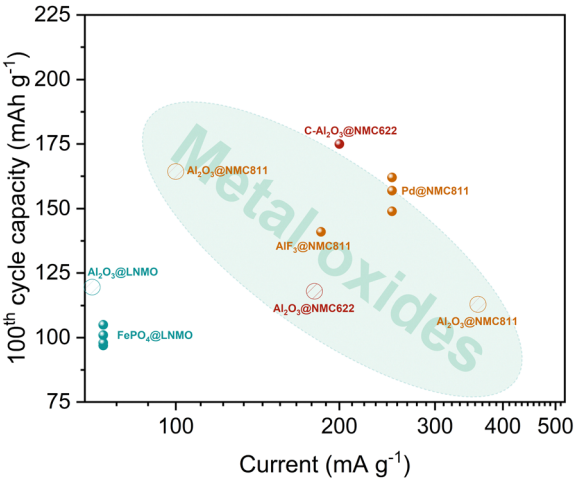

Fig. 10 Specific discharge capacity at the 100th cycle *vs.* discharge current for CAMs coated with phosphates, fluorides, metals, and organic-derived carbon composites *via* powder ALD. Data points for Al_2O_3-coated CAMs are labeled while the highlighted area signifies the best cycling results obtained with metal oxide-based coatings for comparison.

LLO yielded impressive specific capacities of 294 mA h g^{-1} in the 1st cycle and 231 mA h g^{-1} at the 100th cycle using a current rate of C/3 (1C = 250 mA g^{-1}). In another study, NMC622 was exposed to alternating pulses of TMA and fumaric acid vapors, followed by pyrolysis at 600 °C in Ar, resulting in carbon-doped Al_2O_3 coatings that significantly improved the electronic conductivity of the CAM.[115] This method demonstrated substantial enhancements in the reversible capacity and cycling stability of the ALD–MLD modified NMC622 compared to bare, Al_2O_3-coated, and post-annealed Al_2O_3-coated NMC622. For a more comprehensive discussion of the application of ALD–MLD in LIBs, the readers are referred to the work of Meng[162] and Zhao *et al.*[17]

Due to the unavailability of some essential electrochemical data or cycling under non-standard conditions, only a few selected CAMs were chosen for direct comparison with each other and with Al_2O_3-coated CAMs, as shown in Fig. 10. Based on the analysis, the efficiency ranking for non-oxide coatings is as follows (in descending order): ALD–MLD coatings, metals, fluorides, and phosphates. Notably, the ALD–MLD method, especially with subsequent pyrolysis, shows significant promise for simultaneously protecting and enhancing the electrical conductivity of CAMs. In contrast, phosphate coatings demonstrated lower efficiency, even underperforming compared to Al_2O_3-coated LNMO, thereby setting low expectations for future research on phosphate coatings.

2.2 Electrode ALD coating

The commonly used surface coating techniques for cathode materials, including wet chemistry and dry coating, are typically applicable only to CAMs in powder form.[11] As mentioned in Section 1.2, direct coating on the composite electrode (electrode ALD) has been steadily gaining attention in the field

of battery material modification.[163] In this manner, ALD is considered to be a highly suitable coating technique since it allows conformal coating on complex substrates.[51]

Using a relatively low deposition temperature, ALD can develop an artificial CEI by directly forming the coating on the composite electrode surface without deterioration of electrode components.[56,164–166] Fig. 11 exhibits the scheme for electrode ALD-based approaches. Three main types of surface coatings can be obtained which include (1) metal oxide (MO_x), (2) lithiated metal oxide ($Li_xM_yO_z$), and (3) non-oxide coatings, specifically fluoride-based materials. As opposed to powder ALD, the post-annealing route at a high temperature is not common in electrode ALD due to the decomposition temperature limit of the binder.

Despite an obvious disadvantage of less freedom in the development of electrode coatings (limited upscaling and deposition temperature range), the application of electrode ALD is mostly beneficial due to easier processing and less complex optimization procedure. Additionally, compared to powder ALD, electrode ALD can be more advantageous in terms of enhancing the ionic and electronic conductivity. Li^+ mobility and electron transport may be slower when the coating layer is formed on the CAM particles prior to electrode preparation.[166,167] On the contrary, electrode coating may enhance ionic and electronic pathways within the composite material.[123,168,169]

Unlike powder ALD, there are far fewer number of publications available related to electrode ALD. Thus, no cycling duration requirement has been imposed in the selection of literature. The impact of directly applying surface coatings on the composite cathode material to the electrochemical performance, especially cycling stability, is tackled. The corresponding electrochemical data of the modified electrode materials are summarized in Table 3, retrieved from cycling tests performed at room temperature in a half-cell configuration. Similar with powder ALD, some studies did not report the coating thickness.[41,170–175] Moreover, it can also be observed that shorter cycling duration (*i.e.* at most 30–50 cycles) has been imposed in some of the electrode ALD studies examined.[104,165,166,168,171,172,176,177] Due to the limited and varied cycling test data provided by the studies, the capacity retention of the electrode ALD-coated CAM and the corresponding percentage change with respect to the uncoated sample has been reported. In the following sections, different electrode ALD coatings are presented, discussed based on the type of CAM utilized in the composite electrode including LCO, Ni-rich NMC, LLO, LMO, and LNMO.

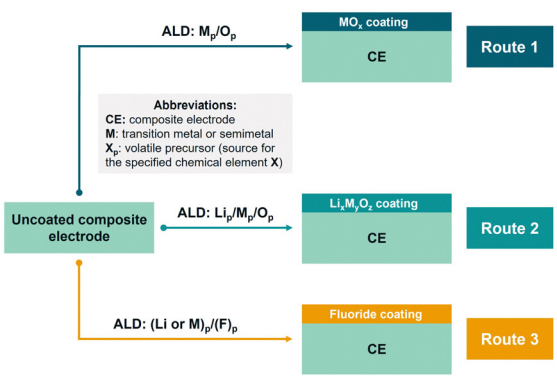

Fig. 11 Scheme of electrode ALD-based approaches to obtain coated composite electrode categorized by the nature of the coating material.

2.2.1 Layered CAMs

2.2.1.1 LCO. As previously discussed, the actual practical capacity of LCO is significantly lower due to cation disorder in the structure and unwanted phase transition at high SOCs. These phenomena result to dissolution of Co into the electrolyte and cracking within the LCO particles.[37,123,171] Several studies have successfully addressed these degradation mechanisms by utilizing electrode ALD to develop a surface coating layer that protects the bulk LCO, leading to an improved electrochemical performance.

Al_2O_3, TiO_2, and ZrO_2 are the most commonly studied ALD metal oxide coatings on LCO electrodes. Li *et al.*[123] conducted a comparative study on the effects of the aforementioned metal oxides on the cycling performance and rate capability of a commercial LCO at a high cutoff of 4.5 V. Upon choosing the optimal thickness (2 ALD cycles), the cycling results show that the electrode ALD coatings can improve the cycling stability of LCO, with Al_2O_3 retaining $\sim$148 mA h g^{-1} and achieving the highest capacity retention after 100 cycles at 1C. Compared with the uncoated sample, the capacity retention increased by 10.7% for TiO_2, 12.6% for ZrO_2, and 23.0% for Al_2O_3-coated LCO. On the other hand, the ZrO_2-coated LCO demonstrates the best rate capability, driven by the coating material's high electrical conductivity.[123]

An earlier work by Cheng *et al.*[171] also cited Al_2O_3 as a better coating material than TiO_2, in terms of improving the cycling performance of LCO, as illustrated in Fig. 12. Based on the band line-up analysis, the study found out that the Al_2O_3 layer does not participate in the redox reactions due to its large band gap, thereby leading to a stable LCO structure during the charge–discharge processes. However, similar with the powder ALD findings, it is important to optimize the coating thickness due to the poor electronic and ionic conductivity of Al_2O_3. Notably, despite the thicker (2–3 nm) Al_2O_3 coating developed on the composite electrode, the capacity retention improved by 71% compared with bare electrode after 45 cycles (Fig. 12). A longer cycling duration is recommended to make reliable conclusions about stability. More Al_2O_3-coated LCO electrode-related studies[74,170,176,178] are listed in Table 3.

While metal oxide ALD coatings have demonstrated their effectiveness in improving the cycling stability of LCO-based LIBs, their instability toward hydrofluoric acid (HF) exposure limits further cycling stability enhancement, especially at high voltage operation. The presence of HF is driven by the reaction between water and lithium salt (*e.g.* $LiPF_6$) in the electrolyte. The formed HF may attack the CAM, resulting to TM dissolution and thickening of CEI.[74] These drawbacks have led to the exploration of metal fluoride-based coatings to address the corrosive effects of HF.[177]

The study of Zhou *et al.*[170] validates the superior cycling stability of a metal fluoride over a metal oxide-based coating

Table 3 Electrochemical performance data of CAMs coated by electrode ALD and tested in half-cell configuration

Active material	Coating material	ALD cycles	Thickness, nm	Current, mA g^{-1}	Working potential	Capacity retention, %	Cycle number	Ref.
LCO	Al_2O_3	2	~0.264	140	3.0–4.5 V	94.0 (▲23.0%)	100	123
	Al_2O_3	2	0.3–0.4	140	3.3–4.5 V	~79.0 (▲39.0%)	120	74
	Al_2O_3	2	0.33–0.66	500	3.3–4.5 V	~100.0 (▲100.0%)	200	178
	Al_2O_3	2	—	160	4.6 V	18.0	100	170
	Al_2O_3	10	2–3	—	2.8–4.5 V	~60.0 (▲56.0%)	50	176
	Al_2O_3	10	2–3	—	3.0–4.5 V	76.0 (▲71.0%)	45	171
	TiO_2	2	~0.224	140	3.0–4.5 V	81.6 (▲10.7%)	100	123
	TiO_2	50	—	—	3.0–4.5 V	71.0 (▲68.0%)	45	171
	ZrO_2	2	~0.256	140	3.0–4.5 V	83.5 (▲12.6%)	100	123
	AlW_xF_y	5	~1	20	2.5–4.4 V	99.0 (▲14.0%)	50	177
	AlF_3	2	—	160	4.5 V	91.0	100	170
	AlF_3	2	—	160	4.7 V	70.0	160	170
NMC532	Al_2O_3	4	~0.44	200	3.0–4.6 V	75.5 (▲15.6%)	100	168
	Al_2O_3	4	~0.44	200	2.0–4.8 V	76.8 (▲18.4%)	30	168
	Al_2O_3	5	0.5–1.5	85	3.0–4.5 V	85.0 (▲10.0%)	100	179
NMC622	Al_2O_3	5	2–4	80	3.0–4.3 V	(▲9.1%)	110	164
	Al_2O_3	10	~1.0	90	3.0–4.3 V	84.9 (▲3.6%)	45	165
	Al_2O_3	10	~1.0	90	3.0–4.5 V	89.7 (▲13.5%)	45	165
	Al_2O_3	10	~1.0	90	3.0–4.7 V	87.8 (▲11.9%)	45	165
	Al_2O_3	20	~2.0	90	3.0–4.3 V	92.0 (▲10.7%)	45	165
	Al_2O_3	20	~2.0	90	3.0–4.5 V	94.5 (▲18.3%)	45	165
	Al_2O_3	20	~2.0	90	3.0–4.7 V	89.5 (▲13.6%)	45	165
	Al_2O_3	40	~4.0	90	3.0–4.3 V	82.3 (▲1.0%)	45	165
	Al_2O_3	40	~4.0	90	3.0–4.5 V	85.3 (▲9.1%)	45	165
	Al_2O_3	40	~4.0	90	3.0–4.7 V	85.9 (▲10.0%)	45	165
	ZrO_2	5	~0.8	90	3.0–4.5 V	86.0 (▲10.0%)	50	166
	ZrO_2	20	~3.2	90	3.0–4.5 V	94.0 (▲18.0%)	50	166
	ZrO_2	40	~6.5	90	3.0–4.5 V	82.0 (▲6.0%)	50	166
	TiO_x	50	3–5	180	3.0–4.4 V	75.0 (▲14.0%)	100	29
	TiO_x	50	3–5	180	3.0–4.6 V	54.0 (▲24.0%)	100	29
	$Li_xTi_yO_z$	10	2–3	180	3.0–4.4 V	82.0 (▲21.0%)	100	29
	$Li_xTi_yO_z$	10	2–3	180	3.0–4.6 V	67.0 (▲37.0%)	100	29
NMC71.51.5	Al_2O_3	5	2–4	80	3.0–4.3 V	(▲14.0%)	110	164
NMC811	Al_2O_3	5	2–4	100	3.0–4.3 V	(▲14.4%)	110	164
	$LiAlF_4$	20	—	50	2.75–4.5 V	76.0	300	41
	LiF	150	13–15	200	3.0–4.6 V	85.0 (▲6.0%)	100	56
LLO	Al_2O_3	2	—	25	2.0–4.8 V	95.6 (▲15.6%)	30	104
	Al_2O_3	10	—	—	2.0–4.6 V	96.2 (▲4.9%)	25	172
	ZnO	5	1.5 ± 0.3	—	2.0–4.8 V	78 (▲10.0%)	80	173
	TiO_2	10	1.5 ± 0.3	—	2.0–4.8 V	94 (▲26.0%)	80	173
	$ZnO–TiO_2$	4/6	1.7 ± 0.4	—	2.0–4.8 V	~97 (▲29.0%)	80	180
	$AlF_3–Al_2O_3$	5/1	—	250	2.0–4.8 V	84 (▲59.0%)	200	174
LMO	Al_2O_3	6	0.9	300	3.4–4.5 V	~95 (▲17.0%)	100	42
	Al_2O_3	6	≤1.0	120	3.4–4.5 V	54.7 (▲5.4%)	100	78
	Al_2O_3	10	~1	148	3.5–4.4 V	~64 (▲38.0%)	500	181
	ZnO	6	~1	120	3.5–4.5 V	~76 (▲26.7%)	100	78
	ZnO	6	~1	120	3.5–4.5 V	~87 (▲1.2%)	100	138
	ZnO	6	1.02	120	3.4–4.5 V	~69 (▲21.0%)	100	137
	TiO_2	15	~1.0	60	3.0–4.5 V	95 (▲5.6%)	140	62
	ZrO_2	6	1.74	120	3.4–4.5 V	70 (▲20.5%)	100	78
	ZrO_2	6	1.74	120	3.4–4.5 V	70 (▲20.0%)	100	139
LNMO	Al_2O_3	10	1.2	70	3.5–5.0 V	91 (▲16.0%)	200	65
	Al_2O_3	6	≤1	73.5	3.5–4.9 V	98 (▲14.0%)	200	182
	$AlPO_4$	10	—	—	3.5–5.0 V	94 (▲25.0%)	100	175

The symbol and corresponding percentage refer to the relative change of the reported value with respect to the uncoated CAM (increased ▲, decreased ▼, not changed ■).

when applied on a free-standing LCO/multiwall carbon nanotube/nanocellulose fibril (LCO-MWCNT-NCF) electrode. Using Li metal as the counter electrode, the cycling stability has been evaluated at different cutoff levels. With 2 ALD cycles of AlF_3, LCO-MWCNT-NCF sustains 75.7% (216 mA h g^{-1} to 163 mA h g^{-1}) of its initial capacity after 100 charge–discharge cycles at 4.7 V. On the other hand, the Al_2O_3-coated LCO-MWCNT-NCF struggles to maintain its performance at a lower cutoff of 4.6 V, losing 82% (149 mA h g^{-1} to 25 mA h g^{-1}) of its initial capacity after 100 cycles. Due to its wide band-gap dieletric, AlF_3 is electrically insulating. Thus, thickness optimization is a crucial parameter in the electrode coating design.[170] The work of Park *et al.*[177] also demonstrates the superior cycling enhancement of a metal fluoride coating, AlW_xF_y, deposited on a LCO electrode using 5 ALD cycles,

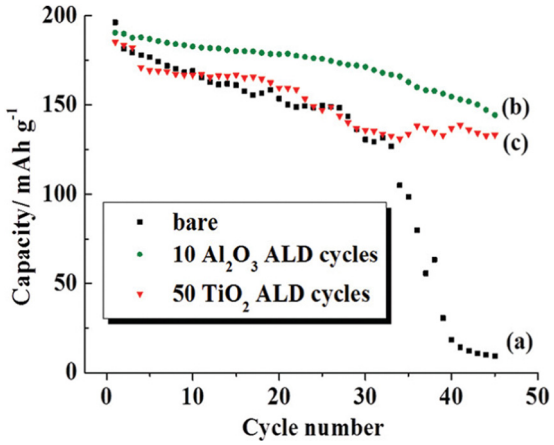

Fig. 12 Comparison of cycling performance of (a) bare, (b) Al_2O_3, and (c) TiO_2-coated LCO electrodes using 10 and 50 ALD cycles, respectively. Reprinted with permission from ref. 171. Copyright 2012 American Chemical Society.

which reported a 99% capacity retention compared with 85% for bare LCO after 50 cycles.

2.2.1.2 Ni-rich NMC. To achieve higher energy density LIBs, the use of Ni-rich NMC and a high cutoff potential are necessary.[11] However, these strategies also accelerate the degradation processes, leading to rapid cell capacity fade.[183] The application of surface coating on Ni-rich NMC *via* electrode ALD aims to lessen the interfacial instabilities faced during cycling.[167] The coating serves as a barrier to lessen the detrimental side reactions that occur between the highly delithiated NMC and the electrolyte.[184] Considering the different NMC compositions and coating materials available, it is crucial to understand the role of the ALD parameters employed in enhancing the electrochemical performance of LIBs.[164] The following discussion will focus on electrode ALD studies that utilized Ni-rich NMC electrodes such as NMC532, NMC622, and NMC811. Lower Ni concentration such as NMC111 are discussed elsewhere.[169,185]

Electrode ALD deposition of Al_2O_3 has also been successfully implemented in NMC532 and NMC622.[165,168,179] In the study of Su *et al.*,[179] the effect of 2, 5, 8, and 10 ALD cycles of Al_2O_3 deposited on a NMC532 electrode have been investigated. A comparison of the TEM images of the uncoated (Fig. 13a) and Al_2O_3-coated (Fig. 13b) NMC532 electrodes confirms the development of a uniform and dense coating with a thickness of 1–3 nm. The study reported that the thickness of Al_2O_3 has a direct influence on the electrical conductivity and Li^+ diffusion, citing 5 ALD cycles to be the most optimal thickness. After 100 cycles at 0.5C (85 mA g^{-1}) from 3.0–4.5 V, the Al_2O_3-coated NMC532 reported 10% higher capacity retention compared to the uncoated sample ($\sim$138 mA h g^{-1} *vs.* $\sim$117 mA h g^{-1}). The coating assisted in reducing the parasitic side reactions at the interface, resulting in lesser R_{ct} growth during cycling. Shi *et al.*[168] also developed Al_2O_3 coating on NMC532 electrode, which was tested up to 4.8 V. As expected, the Al_2O_3-coated electrode exhibits an improved cycling stability compared with

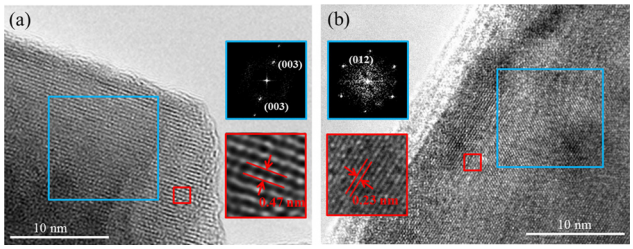

Fig. 13 TEM images of (a) uncoated and (b) Al_2O_3-coated (10 ALD cycles) NMC532. Inset: Corresponding Fast Fourier Transform diagram and lattice fringes. Reprinted with permission from ref. 179. Copyright 2015 American Chemical Society.

the uncoated sample. At 3.0–4.6 V, the Al_2O_3-coated NMC532 delivers a 75.5% (182 mA h g^{-1} to 137 mA h g^{-1}) capacity retention compared to 59.9% (198 mA h g^{-1} to 116 mA h g^{-1}) for the uncoated electrode, after 100 cycles at 1C. Due to the more severe parasitic side reactions occurring between the highly delithiated NMC532 and the electrolyte, the capacity retention at the 30th cycle with 4.8 V cutoff potential is already comparable to the 100th cycle capacity retention when the cutoff potential is 4.6 V. Nonetheless, Al_2O_3 coating still protects the electrode material from direct contact with the electrolyte, thereby suppressing irreversible side reactions.

Wang *et al.*[165] investigated the effect of different Al_2O_3 coating thicknesses on the cycling performance of NMC622 electrode when tested at different cutoff potentials. In all the cycling windows tested, the sample with 2 nm Al_2O_3 (ALD-20; 20 ALD cycles) reported the highest capacity retention values after 45 cycles at 92.0%, 94.5%, and 89.5% for 4.3, 4.5, and 4.7 V cutoff, respectively. The R_{ct} for bare NMC622 increases as the cycling window increases, resulting in decreasing capacity retention of 81.3%, 76.2%, and 75.9% for 4.3, 4.5, and 4.7 V cutoff, respectively. Interestingly, the harsh operation at 4.7 V did not severely impact the reversible capacity of the Al_2O_3-coated NMC622, which reported the highest discharge capacity of $\sim$177 mA h g^{-1} at the 45th cycle. Liu *et al.*[166] also demonstrated the importance of determining the optimal coating thickness in improving capacity retention in their study of ZrO_2-coated NMC622 electrodes. The study reported that the ideal coating thickness should be $\sim$3.2 nm (20 ALD cycles), which exhibited a 94% capacity retention compared with bare NMC622 at 76%, after 50 cycles at 0.5C. A lower thickness value might be too thin to protect the NMC622 cathode material but a thicker coating might impede the Li^+ mobility and result in lower discharge capacity.[166] Unfortunately, a direct comparison with the ZrO_2-coated NMC622 by powder ALD is not plausible due to the difference in discharge current employed. An extended cycling period can help provide more information about the impact of coating thickness and testing parameters to the efficacy of the Al_2O_3 and ZrO_2 coatings.

The development of lithium-containing coating materials, especially those with relatively higher Li^+, can address the concern regarding lower initial capacity performance, brought about by the relatively poor ionic and electronic conductivity of

metal oxide-based coatings. The study of Ahaliabadeh *et al.*[29] compared the electrochemical performance of NMC622 electrodes coated with TiO_x (TO) and $Li_xTi_yO_x$ (LTO) *via* electrode ALD. It highlights the higher Li^+ diffusivity that occurs in the LTO-coated electrode, which provides better reversibility due to smoother Li^+ intercalation/deintercalation. LTO-coated NMC622 (2–3 nm; 10 ALD supercycles) exhibits an improved capacity retention compared with bare at both cutoff potential of 4.4 V (by 21%) and 4.6 V (by 37%). TO-coated NMC622 (23–5 nm; 50 ALD cycles) was found to be more stable than bare but still lost more capacity during long-term cycling compared with LTO. These results confirm that the utilization of Li-containing surface coating can provide better Li^+ mobility due to the higher conductivity provided by the coating structure.[29] An *in situ* dilatometry test shows that the bare NMC622 experiences a large irreversible height change during the initial cycling, which can lead to severe mechanical deformations within the composite electrode. This result is supported by the post-mortem analysis wherein less microcracks are observed in the coated-NMC622.[29]

Recent electrode ALD modifications on the Ni-rich NMC811 have been focused on metal fluorides including $LiAlF_4$ and LiF.[41,56] These type of coating materials are also desirable in surface coating modification application due to their electrochemical inertness, chemical stability, and Li^+ conductivity. The study of Xie *et al.*[41] shows that having a stable and Li^+ conductive interfacial layer is advantageous when it comes to improving cell performance. At 2.75–4.5 V, the bare NMC811 suffered 29% capacity loss at 113 cycles while the $LiAlF_4$-coated NMC811 passed 300 cycles before experiencing 24% capacity loss. Lithium fluoride (LiF) is a byproduct of the electrolyte decomposition and is one of the main components in the CEI. It is beneficial as a coating when utilizing high-voltage operation since it has a wide stable operating window.[56] However, LiF has a relatively low Li^+ conductivity. The work of Llanos *et al.*[56] underscores the advantage of utilizing ALD as it can control the uniformity and thickness to allow the formation of a coating without significantly impeding charge transfer at the electrode–electrolyte interface. Uncoated and LiF-coated NMC811 electrodes were evaluated at a high cutoff potential of 4.6 V at 1C (200 mA g^{-1}). Notably, the 13–15 nm LiF coating assisted in retaining 161 mA h g^{-1} after 100 cycles. Compared with uncoated NMC811, the capacity retention improved by 6% which is ascribed to the reduced detrimental side reactions between NMC811 and the electrolyte, helping minimize impedance growth and active material loss.[56]

Overall, the electrode ALD studies on Ni-rich NMC demonstrated the enhancement of capacity retention, regardless of the type of coating. Interestingly, even with the higher number of ALD cycles employed compared with powder ALD, remarkable cycling stability enhancements are observed. Therefore, it is recommended to utilize lower ALD cycle numbers, especially for the metal fluoride-based coatings, and evaluate if this can improve Li^+ kinetics and further enhance the cycling performance.

2.2.1.3 LLO. Several electrode ALD coatings have been investigated to address voltage fading in LLOs, including Al_2O_3,[104,172,174,186,187] $LiAlO_x$,[186] ZrO_2,[186] TiO_2,[173,186] ZnO,[173] and AlF_3.[174] In the study by Jung *et al.*,[104] the application of 6 ALD cycles of Al_2O_3 on $Li[Li_{0.2}Mn_{0.54}Ni_{0.13}Co_{0.13}]O_2$ electrode resulted in enhanced cycling performance, delivering a capacity of ~220 mA h g^{-1} after 30 cycles at 0.1C in a 2.0–4.8 V potential window. On the other hand, the bare electrode exhibited only ~192 mA h g^{-1} after 30 cycles. To boost Li^+ conductivity, the coated electrodes were heat treated at 300°C to induce interatomic diffusion between the coating and bulk materials and form more Li^+ conductive phases. After heat treatment, the Al_2O_3-coated electrode exhibited a specific capacity of ~242 mA h g^{-1} after 30 cycles, while the heat-treated bare electrode delivered only ~204 mA h g^{-1}. While in both cases heat treatment led to an increase in capacities, the difference in capacity values was higher for the coated electrode.

The effect of TiO_2 and ZnO coatings on the electrochemical performance of the $Li_{1.2}Mn_{0.6}Ni_{0.2}O_2$ electrode was investigated by Wang *et al.*[173] Interestingly, TiO_2 deposition produces an even and uniform coating with 1.5 nm (10 ALD cycles) thickness, while ZnO deposition (5 ALD cycles) results in a less uniform coating layer, as illustrated in Fig. 14a–c. Both coated samples demonstrate better capacity retention, with TiO_2 and ZnO retaining 94% and 78% of their capacity, respectively, compared to 68% for the pristine sample after 80 cycles at 0.5C in a 2.0–4.8 V potential window (Fig. 14d). Furthermore, the TiO_2-coated sample exhibits enhanced rate capability, with a high initial specific discharge capacity of 242 mA h g^{-1} at 0.04C. The improvement in rate performance is attributed to the lower R_{ct} reported in the EIS measurements, which is due to the pinhole-free nature of the TiO_2 film.[173] By combining the step-by-step ALD deposition of 4 ALD cycles of ZnO followed by 6 ALD cycles of TiO_2, Wang *et al.*[180] obtained a ZnO–TiO_2-coated $Li_{1.2}Mn_{0.6}Ni_{0.2}O_2$ electrode, which exhibited a higher initial specific discharge capacity (240 mA h g^{-1}) compared with the pristine sample (228 mA h g^{-1}), and higher capacity retention (~97% for coated *vs.* ~68% for pristine) after 80 charge–discharge cycles.

Yu *et al.*[174] studied the influence of the dual-coating approach by applying different numbers of Al_2O_3 and AlF_3 ALD cycles in a step-by-step process onto $Li_{1.2}Mn_{0.54}Co_{0.13}Ni_{0.13}O_2$. The LLO electrode with $1AlF_3$–$5Al_2O_3$ coating (1 ALD cycle of AlF_3 followed by 5 ALD cycles of Al_2O_3) exhibited the highest capacity retention of ~84%, compared to 25% for the uncoated electrode after 200 cycles at 1C between 2.0 V and 4.8 V. XPS results indicated the formation of a $LiAlF_4$ film during cycling, which can suppress side reactions between the electrolyte and electrode. The decrease in R_{ct} of the $1AlF_3$–$5Al_2O_3$-coated LLO electrode during the cycling is also due to the formation of a more stable and conductive $LiAlF_4$ film.

It is worth noting that a number of the electrode ALD studies performed on layered CAMs tested the cycling performance in a full cell configuration. The absence of Li metal as the counter electrode allows longer cycling period evaluation due to the lesser deleterious side reactions with the electrolyte and the possibility of Li dendrite formation.[56] Table 4 lists the studies

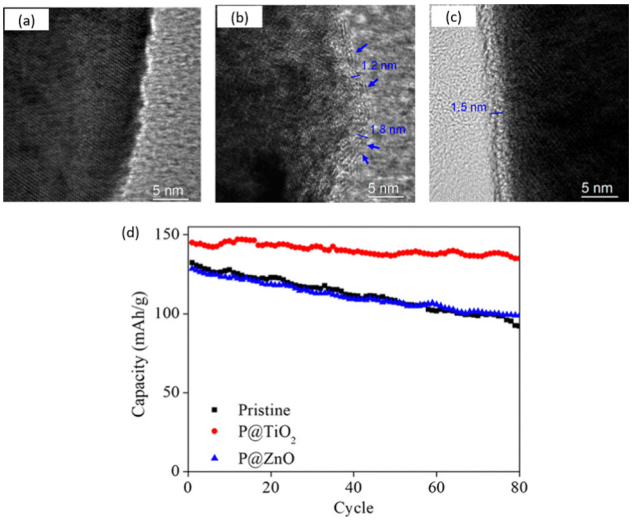

Fig. 14 TEM images of the (a) pristine, (b) ZnO-coated (P@ZnO), and (c) TiO_2-coated (P@TiO_2) $Li_{1.2}Mn_{0.6}Ni_{0.2}O_2$ electrodes and their corresponding (d) cycling performance at 0.5C. Reprinted with permission from ref. 173. Copyright 2018 American Chemical Society.

that also investigated the cycling stability of electrode ALD-coated CAMs using graphite as the counter electrode.

Jung *et al.*[188] further evaluated the efficacy of Al_2O_3 coatings by performing cycling tests in a full-cell configuration. When tested at 3.25–4.45 V *vs.* graphite, the coated electrode delivered 42% higher capacity retention than bare LCO after 100 cycles. The Al_2O_3 electrode coating (0.2–0.3 nm) protects the bulk LCO from undesirable reactions with the electrolyte which may lead to active material dissolution.[188] Ahn *et al.*[167] evaluated the full-cell cycling stability of ZrO_2-coated NMC532 at a high cutoff potential of 4.6 V *vs.* graphite. After 100 cycles at 0.5C, bare NMC532 reported a capacity retention of 71.6% while the ZrO_2 coated samples deliver 77.6% and 73.4% capacity retention for 5 (0.25 nm) and 20 (1.0 nm) ALD cycles, respectively. The thicker coating yields a higher resistance due to the longer Li^+ diffusion pathway. Moreover, even at a faster C rate of 1C, the ZrO_2-coated NMC532 showed a higher capacity retention of 77.4% compared with bare NMC532 at 61.6%. As a HF scavenger, ZrO_2 helps curb active material dissolution. This is supported by the appearance of ZrF_4 peak in the F 1s spectra of the cycled NMC532 electrode.[167] Neudeck *et al.*[66] evaluated the cycling stability of Al_2O_3-coated NMC622 electrodes against graphite anodes. The study demonstrated similar cycling performances for 4-ALD (~0.5 nm) and 10-ALD (~1.3 nm) cycles of Al_2O_3, which reported 126.5 mA h g^{-1} and 127.2 mA h g^{-1} specific discharge capacity, respectively, after 1400 cycles. A 3.2–3.7% increase in capacity retention is achieved by the Al_2O_3-coated NMC622 electrodes compared with the uncoated sample. Bare and LiF-coated NMC811 (13–15 nm) electrodes were evaluated at a high cutoff potential of 4.5 V *vs.* graphite at 1C (200 mA g^{-1}) for 500 cycles. The LiF-coated NMC811 retained 147 mA h g^{-1}, which is 6% higher in capacity retention compared with the bare after long-term cycling.[56]

2.2.2 Spinel CAMs

2.2.2.1 LMO. In order to address capacity fading of a LMO cathode material during cycling, amphoteric oxides that act as HF scavengers and form stable artificial interfaces were employed.[42,62,181,189] The effect of ultrathin conformal Al_2O_3 coating by electrode ALD with various thicknesses (0.6, 0.9, and 1.2 nm) on LMO cathode performance have been investigated by Guan *et al.*[42] The electrode with 0.9 nm (6 ALD cycles) thick Al_2O_3 coating exhibited superior cycling performance, delivering an initial capacity of 101.5 mA h g^{-1} and maintaining a capacity of 96.5 mA h g^{-1} after 100 cycles within a voltage range of 3.4–4.5 V at 2.5C. In contrast, the bare electrode's capacity declined from an initial value of 100.6 mA h g^{-1} to a mere 78.6 mA h g^{-1} at the 100th cycle. The study revealed a critical threshold for coating thickness. The electrode coated with a 1.2 nm (8 ALD cycles) thick Al_2O_3 layer demonstrated the lowest initial capacity (~75 mA h g^{-1}), which was attributed to a significant decrease in the electronic conductivity of the active material, leading to slower charge–discharge kinetics and a noticeable capacity loss. At the same time, the electrode with 0.6 nm (4 ALD cycles) Al_2O_3 coating delivered a capacity of 85.6 mA h g^{-1} at the 100th cycle, due to insufficient protection of the active material by extremely thin coating. Thus, these results underscore the critical role of precise coating thickness in enhancing the cycling performance of LMO electrodes.

The resistive nature of 1 nm thick Al_2O_3 coating was further studied using a 100 nm LMO electrode as a model.[190] The study revealed that the coating effectively postponed the onset of irreversible Li loss, shifting the critical potential up to 4.4 V. This finding suggests that the Al_2O_3 layer enhances surface stability by mitigating premature oxidation. Authors concluded

Table 4 Electrochemical performance data of layered CAMs coated by electrode ALD and tested in full cell configuration

Active material	Coating material	Thickness, nm	Current, mA g^{-1}	Working potential anode; range	Capacity retention, %	Cycle number	Ref.
LCO	Al_2O_3	~0.2–0.3	140	Graphite; 3.25–4.45 V	89.0 (▲42.0%)	100	188
NMC532	ZrO_2	~0.25	—	Graphite; 2.7–4.6 V	77.6 (▲6.60%)	100	167
	ZrO_2	~1.0	—	Graphite; 2.7–4.6 V	73.4 (▲1.8%)	100	167
NMC622	Al_2O_3	~0.5	160	Graphite, 2.8–4.2 V	85.3 (▲3.7%)	1400	66
	Al_2O_3	~1.3	160	Graphite, 2.8–4.2 V	84.8 (▲3.2%)	1400	66
	TiO_x	~3–5	180	Graphite; 3.0–4.4 V	80.0 (▲20.0%)	200	29
	$Li_xTi_yO_z$	~2–3	180	Graphite; 3.0–4.4 V	83.0 (▲23.0%)	200	29
NMC811	LiF	~13–15	200	Graphite; 2.8–4.5 V	87.0 (▲6.0%)	500	56

The symbol and corresponding percentage refer to the relative change of the reported value with respect to the uncoated CAM (increased ▲, decreased ▼, not changed ■).

that the 1 nm Al_2O_3 coating does not suppress CEI layer formation and introduced an additional rate-limiting step, potentially impeding Li^+ movement and overall electrode performance. In a separate study, Waller *et al.*[181] also proved the importance of coating thickness tuning using Al_2O_3 ALD coating on LMO coated-carbon fiber electrodes. The study revealed that LMO electrode with thinner Al_2O_3 coating ($\sim$1 nm; 10 ALD cycles) delivered a 2.5 times greater capacity retention than the uncoated LMO after 500 cycles at 1C. On the contrary, a LMO electrode with a thicker Al_2O_3 coating (5.1 nm; 50 ALD cycles) exhibited comparable capacity retention to the thinner coating after only 300 cycles. The rate capability test also demonstrated the superior behavior of the electrode with the thinner coating, which retained 99.1% of the original C/5 capacity after cycling at higher C rates (10C) and returning to C/5, compared to 93.5% for the uncoated LMO electrode. The ALD coating was suggested to act as a protective barrier against electrolyte degradation, forming aluminum-oxy-fluoride compounds that scavenged HF from the electrolyte, further enhancing electrode longevity and performance.

ZnO is a promising alternative to Al_2O_3 coating, which enhances the specific capacity and capacity retention of LMO electrodes, both at room temperature and at 55 °C.[78,137] When comparing ZnO with other metal oxide coatings, Zhao *et al.*[78] showed that ZnO-coated LMO outperforms both ZrO_2 and Al_2O_3-coated LMO, exhibiting 76.1% capacity retention after 100 cycles at 25 °C and 55 °C. At 55 °C, the conductivity of metal oxides and Li^+ diffusion rate are improved, leading to higher specific capacity of coated LMO electrodes. The ZnO-coated LMO demonstrated the highest initial specific capacity of 84.9 mA h g^{-1}, compared to 80.4 mA h g^{-1} and 79.0 mA h g^{-1} of ZrO_2 and Al_2O_3-coated LMO, respectively. The enhanced cycling performance at elevated temperatures is important, as higher temperatures generally accelerate Mn dissolution and electrolyte decomposition.[78] The correlation between coating thickness and cycling performance is also observed for ZnO coating. Ultrathin ZnO coating (0.34 nm) showed negligible protective effects, delivering capacity retention of 69% and 53% after 100 cycles at 25 °C and 55 °C, respectively.[137] At the same time, thicker ZnO coating (1.07 nm) was found to impede Li^+ diffusion. Even higher capacity retention was achieved by coating a LMO/graphene composite electrode with 6 ALD cycles of ZnO.[138] The resulting ZnO-coated LMO/graphene electrode demonstrated the highest initial discharge capacity of 142 mA h g^{-1} and the highest capacity retention of 86.5% after 100 cycles at 1C and upper cutoff of 4.5 V. On the other hand, bare LMO/graphene electrode delivered 135 mA h g^{-1} at the 1st cycle, and exhibited 85.1% capacity retention after 100 cycles.

Although only an ultrathin layer ($\leq$1 nm) of Al_2O_3 and ZnO can provide sufficient protection against undesired side reactions without aggravating the kinetics, a 5 nm layer of TiO_2 is still a suitable coating for LMO electrode to protect the cathode from surface degradation and Mn dissolution while avoiding significant kinetic barrier to Li^+ movement. Mattelaer *et al.*[190] used 100 nm LMO electrode as a model to coat with 5 nm of TiO_2 by electrode ALD. The TiO_2-coated LMO displayed better kinetics after overcharging to 4.5 V *vs.* Li/Li^+, as evidenced by the sharper and less separated peaks in the cyclic voltammograms compared to an uncoated LMO and LMO coated with 1 nm layer of Al_2O_3. On the contrary, Zhang *et al.*[62] demonstrated the deterioration of Li^+ diffusion when the TiO_2 coating thickness on LMO electrode was about 2.6 nm. At 25 °C, the coated LMO electrode with 40 ALD cycles of TiO_2 exhibited the lowest initial discharge capacity of $\sim$95 mA h g^{-1}, while the LMO electrode coated with 15 ALD cycles (1 nm) of TiO_2 delivered about 128 mA h g^{-1} (Fig. 15a). With the optimal thickness of 1 nm, the TiO_2-coated LMO electrode achieved remarkable capacity retention of 95% after 150 cycles at 0.5C in a voltage range of 3.0–4.5 V. This result is attributed to the protective properties of uniform TiO_2 layer against electrolyte side reactions at the LMO surface. At elevated temperatures (55 °C), the LMO electrode with optimal coating maintained 62.4% capacity retention after 150 cycles, outperforming uncoated LMO electrodes at 56.1% (Fig. 15b). This improvement is suggested to stem from the ability of TiO_2 to mitigate Mn dissolution, which is particularly crucial at higher temperatures where $LiPF_6$ decomposition accelerates HF production.

2.2.2.2 LNMO. Al_2O_3 has also been utilized as an ALD coating deposited directly on a LNMO composite electrode. Fang *et al.*[65] examined the effect of Al_2O_3 coating thickness on the cycling stability of a LNMO electrode by varying the number of ALD cycles (3, 10 and 30). Based on preliminary tests at 25 °C and 55 °C, the LMNO coated with 10 ALD cycles ($\sim$1.2 nm) demonstrated the best cycling performance. This coating thickness was determined as a sweet spot between enhancing the electrochemical performance and minimizing inhibition of Li^+ and electron transport kinetics. In a half-cell configuration, LNMO coated with 10 ALD cycles maintained 91% of its initial capacity compared to 75% capacity retention of the uncoated LMNO after 200 charge–discharge cycles at 0.5C in a voltage range of 3.5–5 V. At an extended cycling period of over 900 cycles, the Al_2O_3-coated electrode exhibited superior performance, delivering 63% capacity retention. The authors attribute the improved performance to the protective effect of the Al_2O_3 layer, which shields LNMO from undesirable side reactions during cycling, including HF etching and active material dissolution.

In order to fully understand the mechanism behind the improved cycling performance due to the ultrathin Al_2O_3 coating, Fang *et al.*[191] employed a dual approach using ensemble-averaged soft X-ray absorption spectroscopy (XAS) at the electrode level and nanoscale scanning transmission electron microscopy-electron energy loss spectroscopy (STEM-EELS) on the surface at the particle level. To investigate the cumulative effect during long-term cycling, both uncoated and Al_2O_3-coated (10 ALD cycles) LMNO electrodes were cycled at 0.2C between 3.5–5.0 V for 35 cycles before XAS measurements. Even after 35 cycles, the Al_2O_3-coated electrode exhibited higher capacity retention (98.8%) compared to the uncoated electrode (97%), as evidenced by the higher overpotential evolution observed for the uncoated LMNO. The comprehensive analysis revealed that

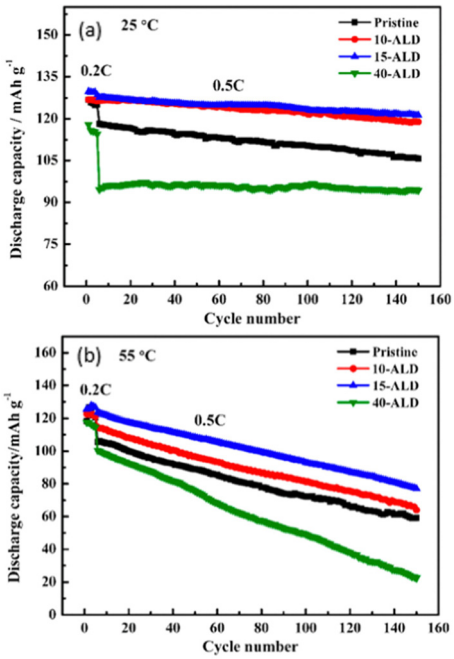

Fig. 15 Comparison of cycling performance of pristine and TiO_2-coated electrodes using different ALD cycles at (a) 25 °C and (b) 55 °C. Reprinted with permission from ref. 62. Copyright 2018 American Chemical Society.

the Al_2O_3 ALD coating suppresses Mn^{2+} evolution and reduces impedance buildup, resulting in less capacity fading. Another study also reported the reduction of the undesired reaction between the LNMO surface and the organic component of electrolyte, achieved by Al_2O_3 ALD coating.[182] In this work, the electrode with only 4 Al_2O_3 ALD cycles (0.4 nm) retained more than 92% of its original capacity compared to 84% capacity retention of the uncoated material after 200 cycles at 0.5C tested between 3.5–4.9 V. After 500 cycles, the surface chemistry of both electrodes was studied by XPS, which reported that the surface of the Al_2O_3-coated electrode carries a lower amount of oxygen-containing organic layer. Therefore, the main effect attributed to the Al_2O_3 ALD coating is the protection of the LNMO surface from undesired side reactions occurring at the electrode–electrolyte interface,[182] including minimizing dissolved metal species,[65,191–193] and HF etching.[65]

Deng *et al.*[175] developed an $AlPO_4$ coating for LNMO electrodes *via* ALD. The LNMO electrode coated with 10 ALD cycles of $AlPO_4$ delivered a lower initial specific discharge capacity of 100.6 mA h g^{-1} but exhibited high capacity retention of 74.9% when cycled at 0.5C in a 3.5–5.0 V potential window for 350 cycles. In comparison, the uncoated LNMO electrode showed an initial specific discharge capacity of 116.3 mA h g^{-1} but had a lower capacity retention of 45.1%. Based on synchrotron X-ray absorption near edge structure (XANES) and XPS results, it was hypothesized that ALD $AlPO_4$ coating can serve not only as an inhibitor of Mn dissolution, but also can transform into a stable CEI layer during cycling. This layer prevents electrolyte decomposition and protects the LNMO structure. Another phosphate-based coating was applied by ALD onto the LNMO surface. Hallot *et al.*[194] developed a nanometer-thick Li_3PO_4 layer coating *via* ALD onto a sputtered LNMO film. Specifically, a 500 nm thick LNMO film with 50 ALD cycles (3 nm) of Li_3PO_4 coating extended the cycling lifetime by 6.5 times longer. During cycling at 1C (4.4–4.8 V), the uncoated sample failed after 180 cycles, whereas the coated sample showed a prolonged life of up to 850 cycles. Although the coating layer was believed to help with preventing undesired surface reactions of LNMO films and improving the lifetime of the electrode, it was difficult to avoid mechanical degradation of the LNMO during cycling.

3 Summary and perspective

Based on a large collection of data analyzed in this review article, ALD is proven to be an effective technique in developing coating layers on the surface of cathode materials to enhance the electrochemical performance, specifically cycling stability, of LIBs. The ALD coatings, whether formed directly on a powder active material or composite electrode, acted as a protective layer between the bulk electrode and electrolyte, thereby reducing harmful side reactions at the interface and active material dissolution into the electrolyte. In this work, the unique characteristics of ALD and its benefits in cathode material modification have been highlighted, which include the following:

- Possibility of deposition on various porous substrates which allows either active material powder or composite electrode coating;
- Ability to control the coating thickness at a nanometer level, which is crucial in ensuring enough barrier layer is formed to protect the bulk electrode without significantly impeding Li^+ transport;
- Suitability for many types of coating materials, such as metal oxides, metal fluorides, and Li-containing mixed oxides, making ALD a versatile technique for developing new coating materials.

On the basis of the surface coatings examined, whether *via* powder ALD or electrode ALD, it can be concluded that metal oxides are the most studied ALD coating material types for intercalation cathodes. Specifically, Al_2O_3 is the most frequently used ALD coating material nowadays. The low cost of different precursors, and the possibility to use moderate temperatures for deposition make it easy to employ this material as a coating. However, the electrochemical enhancement is limited by its low ionic and electronic conductivity. Thus, other metal oxide based materials are gaining popularity as well due to their higher conductivity such as ZrO_2, TiO_2, ZnO, and CeO_2. In general, these coating materials are good protective layers to enhance interfacial stability, leading to better cycling performance.

In comparing the results of powder coatings, it can be surmised that the development of new coatings based on a single p- or d-block metal oxides has likely reached its peak. This is evident from the fact that Al_2O_3-coated materials perform comparably, and often better, than those coated with rarer

oxides. Therefore, future efforts should focus on multi-metal and post-processed oxides, as well as non-oxide-based coatings. Of particular interest are Li-containing mixed oxides, which can be obtained either directly through ALD with a Li precursor or *via* post-heating of a single metal oxide coated active material. The latter process promoted lithiation of the coating material and surface doping. Another promising approach involves a two-stage process: first coating a hydroxide precursor of the active electrode material with a metal oxide, followed by high-temperature lithiation, which also results in Li-containing coatings and surface dopings. Additional methods, such as metal nanoparticle coatings and ALD–MLD, which promoted the cathode materials specific capacity above the metal oxides level, also warrant further exploration. On the other hand, the investigation of metal oxide-based coatings for electrode ALD is still growing as this process is found more favorable in terms of enhancing ionic and electronic pathways. Moreover, the recent works on metal fluorides also bring promising results, mainly due to their electrochemical stability compared to metal oxide-based coatings.

The comparison of powder *versus* electrode ALD coatings revealed a consistently higher value of the optimized coating thickness in the latter process, which is expected due to the need to coat the particles embedded deep within the composite electrode structure. Fig. 16 provides a comparison of the cycling performance of Al_2O_3-coated powder active material and composite electrode based on their specific discharge capacity at the 100th cycle. The best results obtained for both substrates are shown, where the highlighted results refer to powder ALD coating of CAM. It can be seen that both approaches produce modified cathodes with similar performance. Aside from ALD parameters, battery assembly and testing conditions vary across the ALD studies tackled in this review article. These include electrolyte composition, separator material, Li metal counter electrode purity, active material loading, cycling mode (*e.g.* constant current or constant current–constant voltage), among others. The challenge of comparing these parameters is a well-known issue in the battery field, stemming from the lack of standardized assembly and testing protocols. Thus, the possibility of directly comparing the cycling behavior for some materials is not possible. Overlap in data obtained for Al_2O_3-coated LMO by powder coating and electrode coating indicates the publication of the same data twice.[42,119] Moreover, the authors did not clearly specify the methods used for coating in these papers. It was later found that in another article, the authors reported the same data for LMO electrode coated by 6 ZnO layers cycled at 55 °C.[78,137]

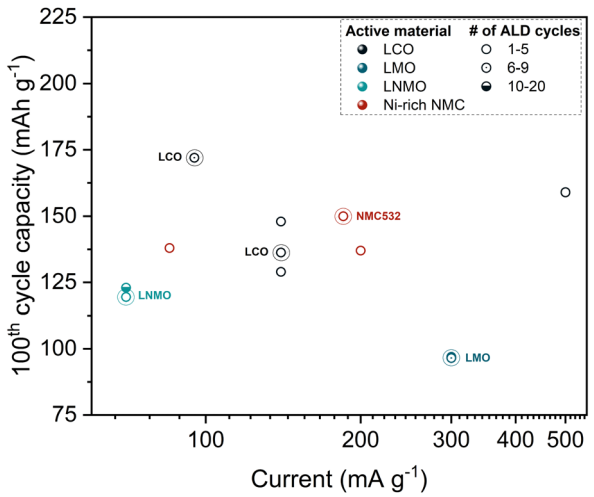

Fig. 16 Specific discharge capacity at the 100th cycle *vs.* discharge current for different CAMs coated with Al_2O_3 *via* powder and electrode ALD. The highlighted data points specify the best cycling results obtained with Al_2O_3 powder coating.

The complexities of and differences in electrochemical testing protocols posed several challenges during the data analysis of the studies considered in this review. The difference in the range of working potential window employed during cycling tests must be noted when comparing results of similar coating materials, as this parameter can substantially affect the electrochemical conditions. Due to the inherent low conductivity and/or the extra layer of diffusion imposed by the coating material, a slightly lower discharge capacity during the first few cycles is sometimes obtained. However, this is compensated by the improvement of performance as the cycling progresses, resulting in higher capacity retention. Additionally, the unavailability of thickness (in Å or nm) data in research articles makes it impossible to assess the specific optimal thickness value. The reported growth rate of the ALD process also varies from study to study (*e.g.* ~1.1 Å for Al_2O_3,[60,93,119] and ~0.36 Å for TiO_2 coating[64,127]). It was observed that recent studies usually report higher specific discharge capacities for the coated material. It should be noted that sometimes the enhanced behavior is due to the improvement in the manufactured reference material, rather than the coating effect.

Author contributions

Princess Stephanie Llanos: conceptualization, formal analysis, project administration, visualization, writing – original draft, writing – review & editing. Alisa R. Bogdanova: conceptualization, formal analysis, project administration, visualization, writing – original draft, writing – review & editing. Filipp Obrezkov: conceptualization, formal analysis, visualization, writing – original draft, writing – review & editing. Nastaran Farrahi: formal analysis, writing – original draft, writing – review & editing. Tanja Kallio: conceptualization, funding acquisition, supervision, writing – review & editing.

Data availability

No primary research results, software or code have been included and no new data were generated or analysed as part of this review.

Conflicts of interest

There are no conflicts to declare.

Acknowledgements

This work acknowledges the financial support from the following organizations: Business Finland the NextGenBat project (grant no. 44811/31/2020), and the European Union, the SOLiD project (grant agreement no. 101069505). Views and opinions however those of the author(s) only and do not necessarily reflect those of the European Union or the European Climate, Infrastructure and Environment Executive Agency (CINEA). Neither the European Union nor the granting authority can be held responsible for them.

References

1 P. A. Østergaard, N. Duic, Y. Noorollahi and S. Kalogirou, *Renewable Energy*, 2023, **219**, 119377.
2 A. M. Adeyinka, O. C. Esan, A. O. Ijaola and P. K. Farayibi, *Sustainable Energy Res.*, 2024, **11**, 26.
3 G. G. Njema, R. B. O. Ouma and J. K. Kibet, *J. Renewable Energy*, 2024, **2024**, 2329261.
4 T. M. Gür, *Energy Environ. Sci.*, 2018, **11**, 2696–2767.
5 Y. Liu, X. Lin, Y. Sun, Y. Xu, B. Chang, C. Liu, A. Cao and L. Wan, *Small*, 2019, **15**, 1901019.
6 M. Lee, W. Ahmad, D. W. Kim, K. M. Kwon, H. Y. Kwon, H.-B. Jang, S.-W. Noh, D.-H. Kim, S. J. A. Zaidi, H. Park, H. C. Lee, M. Abdul Basit and T. J. Park, *Chem. Mater.*, 2022, **34**, 3539–3587.
7 A. Manthiram, *Nat. Commun.*, 2020, **11**, 1550.
8 F. M. N. U. Khan, M. G. Rasul, A. Sayem and N. K. Mandal, *J. Energy Storage*, 2023, **71**, 108033.
9 D. Choi, N. Shamim, A. Crawford, Q. Huang, C. K. Vartanian, V. V. Viswanathan, M. D. Paiss, M. J. E. Alam, D. M. Reed and V. L. Sprenkle, *J. Power Sources*, 2021, **511**, 230419.
10 S. Karimzadeh, B. Safaei, C. Yuan and T.-C. Jen, *Electrochem. Energy Rev.*, 2023, **6**, 1–50.
11 Z. Ahaliabadeh, X. Kong, E. Fedorovskaya and T. Kallio, *J. Power Sources*, 2022, **540**, 231633.
12 J. Lu, Z. Chen, Y. Cui and K. Amine, *Electrochem. Energy Rev.*, 2018, **1**, 35–53.
13 Q. Li, J. Chen, L. Fan, X. Kong and Y. Lu, *Green Energy Environ.*, 2016, **1**, 18–42.
14 X. Wang and G. Yushin, *Energy Environ. Sci.*, 2015, **8**, 1889–1904.
15 J. Liu, B. Li, J. Cao, X. Xing and G. Cui, *J. Energy Chem.*, 2024, **91**, 73–98.
16 W. Lin, W. Bao, J. Cai, X. Cai, H. Zhao, Y. Zhang, Y. Deng, S. Yang, Z. Zhou, Z. Liu and J. Xie, *Appl. Surf. Sci.*, 2023, **615**, 156278.
17 Y. Zhao, L. Zhang, J. Liu, K. Adair, F. Zhao, Y. Sun, T. Wu, X. Bi, K. Amine, J. Lu and X. Sun, *Chem. Soc. Rev.*, 2021, **50**, 3889–3956.
18 J. Ma, J. Sung, Y. Lee, Y. Son, S. Chae, N. Kim, S.-H. Choi and J. Cho, *Adv. Energy Mater.*, 2020, **10**, 1903400.
19 M. Dirican, Y. Lu, K. Fu, H. Kizil and X. Zhang, *RSC Adv.*, 2015, **5**, 34744–34751.
20 S. Yang, P. Yan, W. Bao, H. Zhu, X. Cai, L. Zhao, Y. Zhang, W. Lin, Y. Deng, Y. Wu and J. Xie, *ACS Energy Lett.*, 2023, **8**, 4278–4286.
21 Y. Tesfamhret, H. Liu, Z. Chai, E. Berg and R. Younesi, *ChemElectroChem*, 2021, **8**, 1516–1523.
22 S. Jurng, S. K. Heiskanen, K. W. D. K. Chandrasiri, M. Y. Abeywardana and B. L. Lucht, *J. Electrochem. Soc.*, 2019, **166**, A2721–A2726.
23 M. Dalkilic, A. Schmidt, T. D. Schladt, P. Axmann, J. DuMont, J. Travis, D. Lindblad, L. Kondracki, M. Wohlfahrt-Mehrens, S. Trabesinger and M. Lindén, *J. Electrochem. Soc.*, 2022, **169**, 110537.
24 E. Jin, K. Tantratian, C. Zhao, A. Codirenzi, L. V. Goncharova, C. Wang, F. Yang, Y. Wang, P. Pirayesh, J. Guo, L. Chen, X. Sun and Y. Zhao, *Small*, 2022, **18**, e2203045.
25 L. Chen, K.-S. Chen, X. Chen, G. Ramirez, Z. Huang, N. R. Geise, H.-G. Steinruck, B. L. Fisher, R. Shahbazian-Yassar, M. F. Toney, M. C. Hersam and J. W. Elam, *ACS Appl. Mater. Interfaces*, 2018, **10**, 26972–26981.
26 C.-F. Lin, A. C. Kozen, M. Noked, C. Liu and G. W. Rubloff, *Adv. Mater. Interfaces*, 2016, **3**, 1600426.
27 J. Kim, M. Ku, S. Kim, H. Yang, D. Lee, H. Lee and Y.-B. Kim, *J. Am. Ceram. Soc.*, 2024, **107**, 3134–3145.
28 A. Saha, O. Shalev, S. Maiti, L. Wang, S. H. Akella, B. Schmerling, S. Targin, M. Tkachev, X. Fan and M. Noked, *Mater. Today Energy*, 2023, **31**, 101207.
29 Z. Ahaliabadeh, V. Miikkulainen, M. Mäntymäki, S. Mousavihashemi, J. Lahtinen, L. Yao, H. Jiang, K. Mizohata, T. Kankaanpää and T. Kallio, *ACS Appl. Mater. Interfaces*, 2021, **13**, 42773–42790.
30 C. Guan and J. Wang, *Adv. Sci.*, 2016, **3**, 1500405.
31 W. Li, E. M. Erickson and A. Manthiram, *Nat. Energy*, 2020, **5**, 26–34.
32 Y. Cao, X. Meng and A. Li, *Energy Environ. Mater.*, 2021, **4**, 363–391.
33 Y. Zhao, K. Zheng and X. Sun, *Joule*, 2018, **2**, 2583–2604.
34 B. Ahmed, C. Xia and H. N. Alshareef, *Nano Today*, 2016, **11**, 250–271.
35 S. P. Kühn, K. Edström, M. Winter and I. Cekic-Laskovic, *Adv. Mater. Interfaces*, 2022, **9**, 2102078.
36 K.-X. Wang, X.-H. Li and J.-S. Chen, *Adv. Mater.*, 2015, **27**, 527–545.
37 S. Kalluri, M. Yoon, M. Jo, S. Park, S. Myeong, J. Kim, S. X. Dou, Z. Guo and J. Cho, *Adv. Energy Mater.*, 2017, **7**, 1601507.
38 K. Share, A. Westover, M. Li and C. L. Pint, *Chem. Eng. Sci.*, 2016, **154**, 3–19.
39 M. Qi, L. Wang, X. Huang, M. Ma and X. He, *Small*, 2024, **20**, 2402443.
40 S. Deng, B. Wang, Y. Yuan, X. Li, Q. Sun, K. Doyle-Davis, M. N. Banis, J. Liang, Y. Zhao, J. Li, R. Li, T.-K. Sham, R. Shahbazian-Yassar, H. Wang, M. Cai, J. Lu and X. Sun, *Nano Energy*, 2019, **65**, 103988.
41 J. Xie, A. D. Sendek, E. D. Cubuk, X. Zhang, Z. Lu, Y. Gong, T. Wu, F. Shi, W. Liu, E. J. Reed and Y. Cui, *ACS Nano*, 2017, **11**, 7019–7027.

42 D. Guan and Y. Wang, *Ionics*, 2013, **19**, 1–8.
43 P. Guan, L. Zhou, Z. Yu, Y. Sun, Y. Liu, F. Wu, Y. Jiang and D. Chu, *J. Energy Chem.*, 2020, **43**, 220–235.
44 X. Wang and X.-B. Meng, *Rare Met.*, 2023, **42**, 2121–2156.
45 B. Gupta, M. A. Hossain, A. Riaz, A. Sharma, D. Zhang, H. H. Tan, C. Jagadish, K. Catchpole, B. Hoex and S. Karuturi, *Adv. Funct. Mater.*, 2022, **32**, 2109105.
46 A. S. Asundi, J. A. Raiford and S. F. Bent, *ACS Energy Lett.*, 2019, **4**, 908–925.
47 L. Wen, M. Zhou, C. Wang, Y. Mi and Y. Lei, *Adv. Energy Mater.*, 2016, **6**, 1600468.
48 C. Marichy, M. Bechelany and N. Pinna, *Adv. Mater.*, 2012, **24**, 1017–1032.
49 L. Ma, R. B. Nuwayhid, T. Wu, Y. Lei, K. Amine and J. Lu, *Adv. Mater. Interfaces*, 2016, **3**, 1600564.
50 X. Meng, X.-Q. Yang and X. Sun, *Adv. Mater.*, 2012, **24**, 3589–3615.
51 O. Tiurin and Y. Ein-Eli, *Adv. Mater. Interfaces*, 2019, **6**, 1901455.
52 S. M. George, *Chem. Rev.*, 2010, **110**, 111–131.
53 N. Nitta, F. Wu, J. T. Lee and G. Yushin, *Mater. Today*, 2015, **18**, 252–264.
54 M. Kotal, S. Jakhar, S. Roy and H. K. Sharma, *J. Energy Storage*, 2022, **47**, 103534.
55 Y. Lyu, X. Wu, K. Wang, Z. Feng, T. Cheng, Y. Liu, M. Wang, R. Chen, L. Xu, J. Zhou, Y. Lu and B. Guo, *Adv. Energy Mater.*, 2021, **11**, 2000982.
56 P. S. Llanos, Z. Ahaliabadeh, V. Miikkulainen, J. Lahtinen, L. Yao, H. Jiang, T. Kankaanpää and T. Kallio, *ACS Appl. Mater. Interfaces*, 2024, **16**, 2216–2230.
57 P. K. Nayak, E. M. Erickson, F. Schipper, T. R. Penki, N. Munichandraiah, P. Adelhelm, H. Sclar, F. Amalraj, B. Markovsky and D. Aurbach, *Adv. Energy Mater.*, 2018, **8**, 1702397.
58 E. Hu, X. Yu, R. Lin, X. Bi, J. Lu, S. Bak, K.-W. Nam, H. L. Xin, C. Jaye and D. A. Fischer, *et al.*, *Nat. Energy*, 2018, **3**, 690–698.
59 W. E. Gent, K. Lim, Y. Liang, Q. Li, T. Barnes, S.-J. Ahn, K. H. Stone, M. McIntire, J. Hong and J. H. Song, *et al.*, *Nat. Commun.*, 2017, **8**, 2091.
60 D. Kang, R. E. Warburton, A. U. Mane, J. Greeley and J. W. Elam, *Appl. Surf. Sci.*, 2022, **599**, 153329.
61 M. J. Young, S. Letourneau, R. E. Warburton, W. M. Dose, C. Johnson, J. Greeley and J. W. Elam, *J. Phys. Chem. C*, 2019, **123**, 23783–23790.
62 C. Zhang, J. Su, T. Wang, K. Yuan, C. Chen, S. Liu, T. Huang, J. Wu, H. Lu and A. Yu, *ACS Sustainable Chem. Eng.*, 2018, **6**, 7890–7901.
63 G. Liang, V. K. Peterson, K. W. See, Z. Guo and W. K. Pang, *J. Mater. Chem. A*, 2020, **8**, 15373–15398.
64 H.-M. Cho, M. V. Chen, A. C. MacRae and Y. S. Meng, *ACS Appl. Mater. Interfaces*, 2015, **7**, 16231–16239.
65 X. Fang, M. Ge, J. Rong, Y. Che, N. Aroonyadet, X. Wang, Y. Liu, A. Zhang and C. Zhou, *Energy Technol.*, 2014, **2**, 159–165.
66 S. Neudeck, A. Mazilkin, C. Reitz, P. Hartmann, J. Janek and T. Brezesinski, *Sci. Rep.*, 2019, **9**, 1–11.
67 S. Adhikari, S. Selvaraj and D.-H. Kim, *Adv. Mater. Interfaces*, 2018, **5**, 1800581.
68 J. A. McCormick, B. L. Cloutier, A. W. Weimer and S. M. George, *J. Vac. Sci. Technol., A*, 2007, **25**, 67–74.
69 J. R. Wank, S. M. George and A. W. Weimer, *J. Am. Ceram. Soc.*, 2004, **87**, 762–765.
70 D. Longrie, D. Deduytsche and C. Detavernier, *J. Vac. Sci. Technol., A*, 2013, **32**, 010802.
71 A. Rohatgi, *WebPlotDigitizer*, **https://automeris.io**.
72 Y. Koshtyal, D. Olkhovskii, A. Rumyantsev and M. Maximov, *Batteries*, 2022, **8**, 184.
73 S. Hao and C. Wolverton, *J. Phys. Chem. C*, 2013, **117**, 8009–8013.
74 Y. S. Jung, A. S. Cavanagh, A. C. Dillon, M. D. Groner, S. M. George and S.-H. Lee, *J. Electrochem. Soc.*, 2010, **157**, A75.
75 J. H. Woo, J. E. Trevey, A. S. Cavanagh, Y. S. Choi, S. C. Kim, S. M. George, K. H. Oh and S.-H. Lee, *J. Electrochem. Soc.*, 2012, **159**, A1120–A1124.
76 M. Xie, T. Hu, L. Yang and Y. Zhou, *RSC Adv.*, 2016, **6**, 63250–63255.
77 R. Wu, T. Cao, H. Liu, X. Cheng, X. Liu and Y. Zhang, *ACS Appl. Mater. Interfaces*, 2022, **14**, 25524–25533.
78 J. Zhao and Y. Wang, *J. Solid State Electrochem.*, 2013, **17**, 1049–1058.
79 R. L. Patel, H. Xie, J. Park, H. Y. Asl, A. Choudhury and X. Liang, *Adv. Mater. Interfaces*, 2015, **2**, 1500046.
80 J. W. Kim, D. H. Kim, D. Y. Oh, H. Lee, J. H. Kim, J. H. Lee and Y. S. Jung, *J. Power Sources*, 2015, **274**, 1254–1262.
81 C. A. Kim, H. J. Choi, J. H. Lee, S. Y. Yoo, J. W. Kim, J. H. Shim and B. Kang, *Electrochim. Acta*, 2015, **184**, 134–142.
82 B.-Y. Lee, M. Krajewski, M.-K. Huang, P. Hasin and J.-Y. Lin, *J. Solid State Electrochem.*, 2021, **25**, 2665–2674.
83 E. R. Østli, Y. Tesfamhret, S. Wenner, M. J. Lacey, D. Brandell, A. M. Svensson, S. M. Selbach and N. P. Wagner, *ACS Omega*, 2021, **6**, 30644–30655.
84 B. Zhou, S. An, D. Kitsche, S. L. Dreyer, K. Wang, X. Huang, J. Thanner, M. Bianchini, T. Brezesinski, B. Breitung, H. Hahn and Q. Wang, *Small Struct.*, 2024, **5**, 2400005.
85 Y. Gao, J. Park and X. Liang, *ACS Appl. Energy Mater.*, 2020, **3**, 8978–8987.
86 D. W. Kim, D. Park, C. H. Ko, K. Shin and Y.-S. Lee, *J. Electrochem. Sci. Technol.*, 2021, **12**, 237–245.
87 D. Mohanty, K. Dahlberg, D. M. King, L. A. David, A. S. Sefat, D. L. Wood, C. Daniel, S. Dhar, V. Mahajan, M. Lee and F. Albano, *Sci. Rep.*, 2016, **6**, 26532.
88 J. H. Kim, J.-S. Park, S.-H. Cho, J.-M. Park, J. S. Nam, S.-G. Yoon, I.-D. Kim, J.-W. Jung and H.-S. Kim, *J. Mater. Chem. A*, 2022, **10**, 25009–25018.
89 H. Yu, Y. Gao, J. Kirtley, G. Borgmeyer, X. He and X. Liang, *J. Electrochem. Soc.*, 2022, **169**, 050520.
90 L. David, K. Dahlberg, D. Mohanty, R. E. Ruther, A. Huq, M. Chi, S. J. An, C. Mao, D. M. King, L. Stevenson and D. L. Wood, *ACS Appl. Energy Mater.*, 2019, **2**, 1308–1313.
91 J. Li, J. Xiang, G. Yi, Y. Tang, H. Shao, X. Liu, B. Shan and R. Chen, *Coatings*, 2022, **12**, 84.

92 Z. Li, Z. Zhang, B. Huang, H. Wang, B. He, Y. Gong, J. Jin and R. Wang, *Coatings*, 2022, **12**, 1613.
93 W. Zhu, X. Huang, T. Liu, Z. Xie, Y. Wang, K. Tian, L. Bu, H. Wang, L. Gao and J. Zhao, *Coatings*, 2019, **9**, 92.
94 Y. Chen, M. Wang, J. Chen, J. Yang, Z. Li, Y. Huang, Z. Chen, Y. Zou, J. Zheng and X. Li, *Mater. Lett.*, 2020, **271**, 127771.
95 Y. Shi, Y. Xing, K. Kim, T. Yu, A. L. Lipson, A. Dameron and J. G. Connell, *J. Electrochem. Soc.*, 2021, **168**, 040501.
96 L. A. Riley, S. V. Atta, A. S. Cavanagh, Y. Yan, S. M. George, P. Liu, A. C. Dillon and S. H. Lee, *J. Power Sources*, 2011, **196**, 3317–3324.
97 J. W. Kim, J. J. Travis, E. Hu, K. W. Nam, S. C. Kim, C. S. Kang, J. H. Woo, X. Q. Yang, S. M. George, K. H. Oh, S. J. Cho and S. H. Lee, *J. Power Sources*, 2014, **254**, 190–197.
98 A. L. Hoskins, W. W. McNeary, S. L. Millican, T. A. Gossett, A. Lai, Y. Gao, X. Liang, C. B. Musgrave and A. W. Weimer, *ACS Appl. Nano Mater.*, 2019, **2**, 6989–6997.
99 B. Han, B. Key, A. S. Lipton, J. T. Vaughey, B. Hughes, J. Trevey and F. Dogan, *J. Electrochem. Soc.*, 2019, **166**, A3679–A3684.
100 D. H. Jackson and T. F. Kuech, *J. Power Sources*, 2017, **365**, 61–67.
101 M. R. Laskar, D. H. K. Jackson, Y. Guan, S. Xu, S. Fang, M. Dreibelbis, M. K. Mahanthappa, D. Morgan, R. J. Hamers and T. F. Kuech, *ACS Appl. Mater. Interfaces*, 2016, **8**, 10572–10580.
102 X. Zhang, I. Belharouak, L. Li, Y. Lei, J. W. Elam, A. Nie, X. Chen, R. S. Yassar and R. L. Axelbaum, *Adv. Energy Mater.*, 2013, **3**, 1299–1307.
103 J. Zhao, S. Aziz and Y. Wang, *J. Power Sources*, 2014, **247**, 95–104.
104 Y. S. Jung, A. S. Cavanagh, Y. Yan, S. M. George and A. Manthiram, *J. Electrochem. Soc.*, 2011, **158**, A1298.
105 P. Yan, J. Zheng, X. Zhang, R. Xu, K. Amine, J. Xiao, J.-G. Zhang and C.-M. Wang, *Chem. Mater.*, 2016, **28**, 857–863.
106 X. Zhang, X. Meng, J. W. Elam and I. Belharouak, *Solid State Ionics*, 2014, **268**, 231–235.
107 M. Zhou, J. Zhao, S. Qiu, F. Tian, O. Potapenko, S. Zhong, H. Potapenko and Z. Liang, *Int. J. Electrochem. Sci.*, 2020, **15**, 10759–10771.
108 E. Evenstein, Rosy, S. Haber, H. Sclar, L. Houben, K. Leung, M. Leskes and M. Noked, *Energy Storage Mater.*, 2019, **19**, 261–269.
109 B. Huang, R. Wang, Y. Gong, B. He and H. Wang, *Front. Chem.*, 2019, **7**, 107.
110 Y. Li, C. Wan, Y. Tian, J. Li, C. Yang, W. Zhang, X. Zhang, Z. Hao, Z. Yang, P. Guo, B. Yang, D. Ruan, M. Xie and J. Hu, *Appl. Surf. Sci.*, 2023, **609**, 155162.
111 Y. Li, Z. Shi, B. Qiu, J. Zhao, X. Li, Y. Zhang, T. Li, Q. Gu, J. Gao and Z. Liu, *Adv. Funct. Mater.*, 2023, **33**, 2302236.
112 X. Cai, Z. Wang, Y. Xing, C. Zheng, P. Yan, W. Bao, T. Xie, Y. Hu, Y. Deng, Y. Zhang, Y. Wu, S. Yang, F. Zheng, H. Zhang, Z.-J. Wang and J. Xie, *Nano Lett.*, 2023, **23**, 5770–5778.
113 S. Maiti, H. Sclar, R. Sharma, N. Vishkin, M. Fayena-Greenstein, J. Grinblat, M. Talianker, L. Burstein, N. Solomatin, O. Tiurin, Y. Ein-Eli, M. Noked, B. Markovsky and D. Aurbach, *Adv. Funct. Mater.*, 2021, **31**, 2008083.
114 S. Fang, D. Jackson, M. L. Dreibelbis, T. F. Kuech and R. J. Hamers, *J. Power Sources*, 2018, **373**, 184–192.
115 J. Z. Kong, Y. Chen, Y. Q. Cao, Q. Z. Wang, A. D. Li, H. Li and F. Zhou, *J. Alloys Compd.*, 2019, **799**, 89–98.
116 N. Dannehl, S. O. Steinmüller, D. V. Szabó, M. Pein, F. Sigel, L. Esmezjan, U. Hasenkox, B. Schwarz, S. Indris and H. Ehrenberg, *ACS Appl. Mater. Interfaces*, 2018, **10**, 43131–43143.
117 H. S. Kim, B.-S. Jin, Y. S. Jung, S. Lee, M. Jeon and H.-T. Lim, *IEEE Conference and Expo Transportation Electrification Asia-Pacific (ITEC Asia-Pacific)*, 2016.
118 A. M. Wise, C. Ban, J. N. Weker, S. Misra, A. S. Cavanagh, Z. Wu, Z. Li, M. S. Whittingham, K. Xu, S. M. George and M. F. Toney, *Chem. Mater.*, 2015, **27**, 6146–6154.
119 X. Luan, D. Guan and Y. Wang, *J. Nanosci. Nanotechnol.*, 2012, **12**, 7113–7120.
120 E. Zhao, L. Fang, M. Chen, D. Chen, Q. Huang, Z. Hu, Q. Bo Yan, M. Wu and X. Xiao, *J. Mater. Chem. A*, 2017, **5**, 1679–1686.
121 V. Pimenta, M. Sathiya, D. Batuk, A. M. Abakumov, D. Giaume, S. Cassaignon, D. Larcher and J.-M. Tarascon, *Chem. Mater.*, 2017, **29**, 9923–9936.
122 T. Fu, D. Lu, Z. Yao, Y. Li, C. Luo, T. Yang, S. Liu, Y. Chen, Q. Guo, C. Zheng and W. Sun, *J. Mater. Chem. A*, 2023, **11**, 13889–13915.
123 X. Li, J. Liu, X. Meng, Y. Tang, M. N. Banis, J. Yang, Y. Hu, R. Li, M. Cai and X. Sun, *J. Power Sources*, 2014, **247**, 57–69.
124 M. R. Laskar, D. H. K. Jackson, S. Xu, R. J. Hamers, D. Morgan and T. F. Kuech, *ACS Appl. Mater. Interfaces*, 2017, **9**, 11231–11239.
125 J.-Z. Kong, S.-S. Wang, G.-A. Tai, L. Zhu, L.-G. Wang, H.-F. Zhai, D. Wu, A.-D. Li and H. Li, *J. Alloys Compd.*, 2016, **657**, 593–600.
126 J.-Z. Kong, C. Ren, G.-A. Tai, X. Zhang, A.-D. Li, D. Wu, H. Li and F. Zhou, *J. Power Sources*, 2014, **266**, 433–439.
127 C. Qin, J. Cao, J. Chen, G. Dai, T. Wu, Y. Chen, Y. Tang, A. Li and Y. Chen, *Dalton Trans.*, 2016, **45**, 9669–9675.
128 W. Bao, G. Qian, L. Zhao, Y. Yu, L. Su, X. Cai, H. Zhao, Y. Zuo, Y. Zhang, H. Li, Z. Peng, L. Li and J. Xie, *Nano Lett.*, 2020, **20**, 8832–8840.
129 Y. Li, L. Ben, H. Yu, W. Zhao, X. Liu and X. Huang, *Inorganics*, 2022, **10**, 111.
130 S. Blanga, S. Harsha Akella, M. Tsubery, M. Zysler, S. Taragin and M. Noked, *ChemElectroChem*, 2024, **11**, e202400162.
131 E. R. Østli, M. Ebadi, Y. Tesfamhret, M. Mahmoodinia, M. J. Lacey, D. Brandell, A. M. Svensson, S. M. Selbach and N. P. Wagner, *ChemSusChem*, 2022, **15**, e202200324.
132 B. Xiao, H. Liu, J. Liu, Q. Sun, B. Wang, K. Kaliyappan, Y. Zhao, M. N. Banis, Y. Liu, R. Li, T. Sham, G. A. Botton, M. Cai and X. Sun, *Adv. Mater.*, 2017, **29**, 1703764.

133 R. L. Patel, S. A. Palaparty and X. Liang, *J. Electrochem. Soc.*, 2017, **164**, A6236–A6243.
134 R. L. Patel, Y.-B. Jiang, A. Choudhury and X. Liang, *Sci. Rep.*, 2016, **6**, 25293.
135 Y. Gao, X. He, T. Ma, L. Ma, T. Wu, J. Park and X. Liang, *Electrochim. Acta*, 2020, **340**, 135951.
136 Y. Gao, H. Yu, P. Sandineni, X. He, A. Choudhury, J. Park and X. Liang, *J. Phys. Chem. C*, 2021, **125**, 7560–7567.
137 J. Zhao and Y. Wang, *J. Phys. Chem. C*, 2012, **116**, 11867–11876.
138 S. Aziz, J. Zhao, C. Cain and Y. Wang, *J. Mater. Sci. Technol.*, 2014, **30**, 427–433.
139 J. Zhao, G. Qu, J. C. Flake and Y. Wang, *Chem. Commun.*, 2012, **48**, 8108–8110.
140 J. Zhao and Y. Wang, *Nano Energy*, 2013, **2**, 882–889.
141 Y. He, H. Pham, Y. Gao, R. L. Patel, S. Sarkar, X. Liang and J. Park, *Adv. Theory Simul.*, 2020, **3**, 2000002.
142 Y. Gao, R. L. Patel, K.-Y. Shen, X. Wang, R. L. Axelbaum and X. Liang, *ACS Omega*, 2017, **3**, 906–916.
143 J.-Z. Kong, H.-F. Zhai, X. Qian, M. Wang, Q.-Z. Wang, A.-D. Li, H. Li and F. Zhou, *J. Alloys Compd.*, 2017, **694**, 848–856.
144 Y. Gao, Z. Shang, X. He, T. White, J. Park and X. Liang, *Electrochim. Acta*, 2019, **318**, 513–524.
145 E. Wang, Y. Zhao, D. Xiao, X. Zhang, T. Wu, B. Wang, M. Zubair, Y. Li, X. Sun and H. Yu, *Adv. Mater.*, 2020, **32**, 1906070.
146 M. Madadi, J. Heiska, J. Multia and M. Karppinen, *ACS Appl. Mater. Interfaces*, 2021, **13**, 56793–56811.
147 L. Wang, A. Mukherjee, C.-Y. Kuo, S. Chakrabarty, R. Yemini, A. A. Dameron, J. W. DuMont, S. H. Akella, A. Saha, S. Taragin, H. Aviv, D. Naveh, D. Sharon, T.-S. Chan, H.-J. Lin, J.-F. Lee, C.-T. Chen, B. Liu, X. Gao, S. Basu, Z. Hu, D. Aurbach, P. G. Bruce and M. Noked, *Nat. Nanotechnol.*, 2024, **19**, 208–218.
148 Y. Liu, X. Wang, S. K. Ghosh, M. Zou, H. Zhou, X. Xiao and X. Meng, *Dalton Trans.*, 2022, **51**, 2737–2749.
149 Y. Yang, G. Sun, Q. Zhu, Y. Jiang, W. Ke, P. Wang, Y. Zhao, W. Zhang and Z. Wang, *J. Mater. Chem. A*, 2022, **10**, 24018–24029.
150 O. Tiurin, N. Solomatin, M. Auinat and Y. Ein-Eli, *J. Power Sources*, 2020, **448**, 227373.
151 A. Kraytsberg, H. Drezner, M. Auinat, A. Shapira, N. Solomatin, P. Axmann, M. Wohlfahrt-Mehrens and Y. Ein-Eli, *ChemNanoMat*, 2015, **1**, 577–585.
152 A. Shapira, O. Tiurin, N. Solomatin, M. Auinat, A. Meitav and Y. Ein-Eli, *ACS Appl. Energy Mater.*, 2018, **1**, 6809–6823.
153 S. Haber, N. Solomatin, A. Shapira, T. Bendikov, O. Brontvein, Y. Ein-Eli and M. Leskes, *J. Power Sources*, 2023, **560**, 232693.
154 D. H. K. Jackson, M. R. Laskar, S. Fang, S. Xu, R. G. Ellis, X. Li, M. Dreibelbis, S. E. Babcock, M. K. Mahanthappa, D. Morgan, R. J. Hamers and T. F. Kuech, *J. Vac. Sci. Technol., A*, 2016, **34**, 031503.
155 C. Yang, Y. Li, X. Zhang, J. Xiao, H. Xiong, W. Li, P. Guo, Z. Yang and M. Xie, *Ionics*, 2022, **28**, 4547–4554.
156 B. Xiao, J. Liu, Q. Sun, B. Wang, M. N. Banis, D. Zhao, Z. Wang, R. Li, X. Cui, T.-K. Sham and X. Sun, *Adv. Sci.*, 2015, **2**, 1500022.
157 B. Xiao, B. Wang, J. Liu, K. Kaliyappan, Q. Sun, Y. Liu, G. Dadheech, M. P. Balogh, L. Yang, T.-K. Sham, R. Li, M. Cai and X. Sun, *Nano Energy*, 2017, **34**, 120–130.
158 J. Liang, Y. Zhu, X. Li, J. Luo, S. Deng, Y. Zhao, Y. Sun, D. Wu, Y. Hu, W. Li, T.-K. Sham, R. Li, M. Gu and X. Sun, *Nat. Commun.*, 2023, **14**, 146.
159 W.-B. Li, K. Wu, H. Feng, N. Wang, J.-H. Zhang, J.-J. Wang and X.-F. Li, *Tungsten*, 2022, **4**, 346–355.
160 A. Saha, S. Taragin, Rosy, S. Maiti, T. Kravchuk, N. Leifer, M. Tkachev and M. Noked, *Small*, 2022, **18**, 2104625.
161 Rosy, S. Haber, E. Evenstein, A. Saha, O. Brontvein, Y. Kratish, D. Bravo-Zhivotovskii, Y. Apeloig, M. Leskes and M. Noked, *Energy Storage Mater.*, 2020, **33**, 268–275.
162 X. Meng, *J. Mater. Res.*, 2021, **36**, 2–25.
163 Y. S. Jung, A. S. Cavanagh, L. A. Riley, S.-H. Kang, A. C. Dillon, M. D. Groner, S. M. George and S.-H. Lee, *Adv. Mater.*, 2010, **22**, 2172–2176.
164 R. S. Negi, S. P. Culver, M. Wiche, S. Ahmed, K. Volz and M. T. Elm, *Phys. Chem. Chem. Phys.*, 2021, **23**, 6725–6737.
165 X. Wang, J. Cai, Y. Liu, X. Han, Y. Ren, J. Li, Y. Liu and X. Meng, *Nanotechnology*, 2021, **32**, 115401.
166 Y. Liu, X. Wang, J. Cai, X. Han, D. Geng, J. Li and X. Meng, *J. Mater. Sci. Technol.*, 2020, **54**, 77–86.
167 J. Ahn, E. K. Jang, S. Yoon, S.-J. Lee, S.-J. Sung, D.-H. Kim and K. Y. Cho, *Appl. Surf. Sci.*, 2019, **484**, 701–709.
168 Y. Shi, M. Zhang, D. Qian and Y. S. Meng, *Electrochim. Acta*, 2016, **203**, 154–161.
169 X. Li, J. Liu, M. N. Banis, A. Lushington, R. Li, M. Cai and X. Sun, *Energy Environ. Sci.*, 2014, **7**, 768–778.
170 Y. Zhou, Y. Lee, H. Sun, J. M. Wallas, S. M. George and M. Xie, *ACS Appl. Mater. Interfaces*, 2017, **9**, 9614–9619.
171 H.-M. Cheng, F.-M. Wang, J. P. Chu, R. Santhanam, J. Rick and S.-C. Lo, *J. Phys. Chem. C*, 2012, **116**, 7629–7637.
172 M. Choi, G. Ham, B.-S. Jin, S.-M. Lee, Y. M. Lee, G. Wang and H.-S. Kim, *J. Alloys Compd.*, 2014, **608**, 110–117.
173 C.-C. Wang, J.-W. Lin, Y.-H. Yu, K.-H. Lai, K.-F. Chiu and C.-C. Kei, *ACS Sustainable Chem. Eng.*, 2018, **6**, 16941–16950.
174 H. Yu, Y. Gao and X. Liang, *J. Electrochem. Soc.*, 2019, **166**, A2021.
175 S. Deng, B. Xiao, B. Wang, X. Li, K. Kaliyappan, Y. Zhao, A. Lushington, R. Li, T.-K. Sham, H. Wang and X. Sun, *Nano Energy*, 2017, **38**, 19–27.
176 J.-T. Lee, F.-M. Wang, C.-S. Cheng, C.-C. Li and C.-H. Lin, *Electrochim. Acta*, 2010, **55**, 4002–4006.
177 J. S. Park, A. U. Mane, J. W. Elam and J. R. Croy, *Chem. Mater.*, 2015, **27**, 1917–1920.
178 I. D. Scott, Y. S. Jung, A. S. Cavanagh, Y. Yan, A. C. Dillon, S. M. George and S.-H. Lee, *Nano Lett.*, 2011, **11**, 414–418.
179 Y. Su, S. Cui, Z. Zhuo, W. Yang, X. Wang and F. Pan, *ACS Appl. Mater. Interfaces*, 2015, **7**, 25105–25112.
180 C.-C. Wang, J.-W. Lin, Y.-H. Yu, K.-H. Lai, S.-M. Lee, K.-F. Chiu and C.-C. Kei, *J. Alloys Compd.*, 2020, **842**, 155845.

181 G. Waller, P. Brooke, B. Rainwater, S. Lai, R. Hu, Y. Ding, F. Alamgir, K. Sandhage and M. Liu, *J. Power Sources*, 2016, **306**, 162–170.
182 J. Song, X. Han, K. J. Gaskell, K. Xu, S. B. Lee and L. Hu, *J. Nanopart. Res.*, 2014, **16**, 1–8.
183 S. Wu, X. Zhang, S. Ma, E. Fan, J. Lin, R. Chen, F. Wu and L. Li, *Small*, 2022, **18**, 2204613.
184 H. Gao, J. Cai, G.-L. Xu, L. Li, Y. Ren, X. Meng, K. Amine and Z. Chen, *Chem. Mater.*, 2019, **31**, 2723–2730.
185 A. K. Haridas, Q. A. Nguyen, B. F. Song, R. Blaser and S. L. Biswal, *ACS Appl. Energy Mater.*, 2020, **3**, 456–468.
186 I. Bloom, L. Trahey, A. Abouimrane, I. Belharouak, X. Zhang, Q. Wu, W. Lu, D. P. Abraham, M. Bettge, J. W. Elam, X. Meng, A. K. Burrell, C. Ban, R. Tenent, J. Nanda and N. Dudney, *J. Power Sources*, 2014, **249**, 509–514.
187 M. Bettge, Y. Li, B. Sankaran, N. D. Rago, T. Spila, R. T. Haasch, I. Petrov and D. P. Abraham, *J. Power Sources*, 2013, **233**, 346–357.
188 Y. S. Jung, P. Lu, A. S. Cavanagh, C. Ban, G.-H. Kim, S.-H. Lee, S. M. George, S. J. Harris and A. C. Dillon, *Adv. Energy Mater.*, 2013, **3**, 213–219.
189 D. Guan, J. A. Jeevarajan and Y. Wang, *Nanoscale*, 2011, **3**, 1465–1469.
190 F. Mattelaer, P. M. Vereecken, J. Dendooven and C. Detavernier, *Adv. Mater. Interfaces*, 2017, **4**, 1601237.
191 X. Fang, F. Lin, D. Nordlund, M. Mecklenburg, M. Ge, J. Rong, A. Zhang, C. Shen, Y. Liu, Y. Cao, M. M. Doeff and C. Zhou, *Adv. Funct. Mater.*, 2017, **27**, 1602873.
192 J. S. Park, X. Meng, J. W. Elam, S. Hao, C. Wolverton, C. Kim and J. Cabana, *Chem. Mater.*, 2014, **26**, 3128–3134.
193 W. Li, D. Cheng, R. Shimizu, Y. Li, W. Yao, G. Raghavendran, M. Zhang and Y. S. Meng, *Energy Storage Convers. Mater.*, 2022, **49**, 77–84.
194 M. Hallot, B. Caja-Munoz, C. Leviel, O. I. Lebedev, R. Retoux, J. Avila, P. Roussel, M. C. Asensio and C. Lethien, *ACS Appl. Mater. Interfaces*, 2021, **13**, 15761–15773.